Recent Application of Radionuclides in PET/CT Imaging

Pardis Ghafarian, PhD
Professor

Physicist, PET/CT and Cyclotron Centre Masih Daneshvari Hospital, Shahid Beheshti University of Medical Sciences, Tehran, Iran

Chronic Respiratory Diseases Research Center, National Research Institute of Tuberculosis and Lung Diseases (NRITLD), Shahid Beheshti University of Medical Sciences, Tehran, Iran

F18

Production Method: F-18 is usually produced in a cyclotron through the irradiation of oxygen-18 enriched water (H2^18O) with protons. The reaction is as follows:

$^{18}O(p,n)^{18}F$
Half life:109.771min

Application of PET Tracers in Breast Cancer

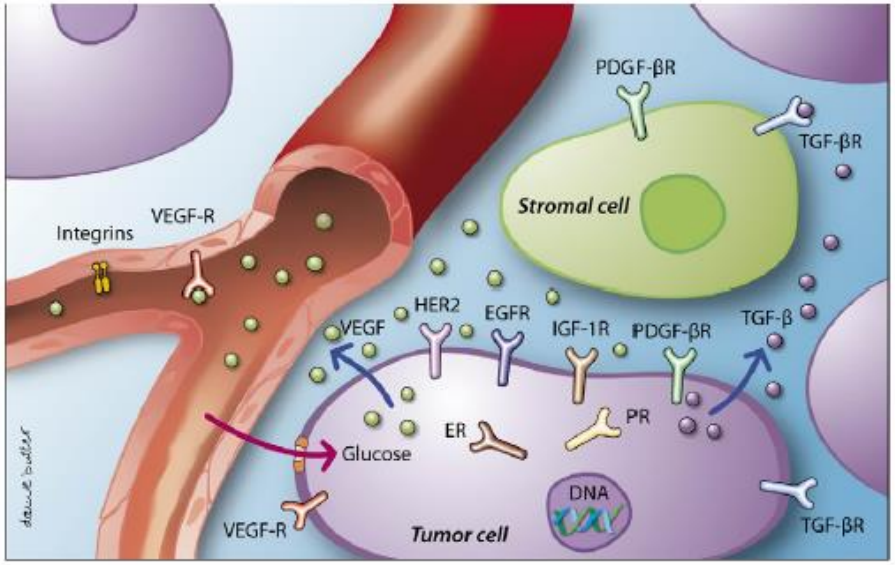

Fig. 1. Schematic presentation of the (potential) targets for breast cancer molecular imaging.

Most clinical data are gathered on the visualization of general processes such as glucose metabolism with the PET-tracer [18F]fluorodeoxyglucose (FDG) and DNA synthesis with [18F]fluoro- L-thymidine (FLT).
Increasingly more breast cancer specific targets are imaged such as the estrogen receptor(Hormone receptor imaging) (ER), growth factors and growth factor receptors. Imaging of the ER with the PET tracer 16-a-[18F]fluoro- 17-b-estradiol (FES) has shown a good correlation between FES tumor uptake and ER density.
111In-trastuzumab SPECT to image the human epidermal growth factor receptor 2 (HER2) showed that in most patients with metastatic HER2 overexpressing disease more lesions were detected than with conventional staging procedures. The PET tracer 89Zr-trastuzumab showed excellent, quantifiable, and specific tumor uptake. 111In-bevacizumab for SPECT and 89Zr-bevacizumab for PET-imaging have been developed for vascular endothelial growth factor (VEGF) imaging as an angiogenic marker. Lastly, tracers for the receptors EGFR, IGF-1R, PDGF-bR and the ligand TGFb are under development.

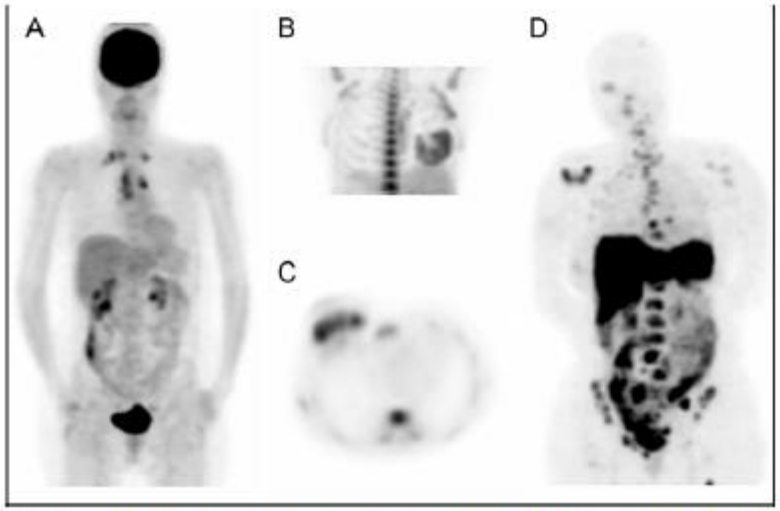

Fig. 2. Examples of three breast cancer patients imaged with various PET tracers. (A) FDG-PET shows physiological FDG uptake in brain, bladder, kidneys, liver, intestine and muscles, and pathological FDG uptake in supraclavicular and mediastinal metastatic lesions. (B,C) FLT-PET shows physiological FLT uptake in liver and bone marrow, and pathological FLT uptake in primary tumor. (D) FES-PET shows physiological FES uptake in liver and intestine, and pathological FES uptake in numerous bone metastases.

2009-Yhe Breast-Munnink

FES

Names: 16α-[18F] Fluoro-17β-estradiol; 16-Fluoroestradiol, 18F-fluoroestradiol

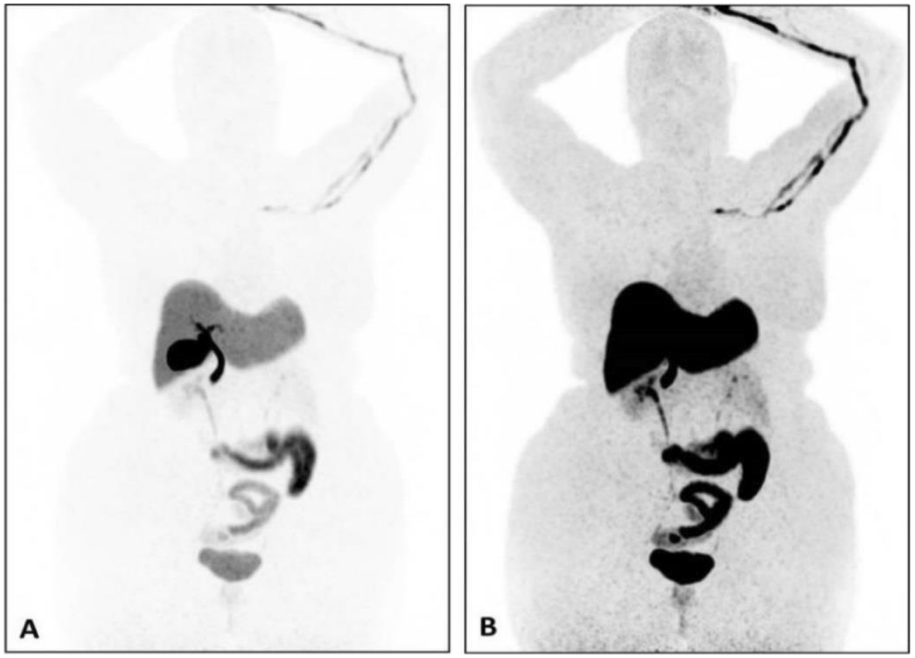

Physiological bio-distribution of 18F-fluoroestradiol. Low (a) and high (b) intensity MIP images

- Treatment with oestrogen receptor antagonists (e.g. tamoxifen, fulvestrant, faslodex, oestrogens) should be suspended for at least 5 weeks prior to performing the scan. Aromatase inhibitors and luteinizing hormone releasing hormone agonists may be continued
- No fasting is required

- 200 MBq of ^{18}F-fluoroestradiol iv
- Level of binding of ^{18}F-FES to the oestrogen receptors remains stable between 20 and 120 min postinjection. For logistical reasons, scanning procedure should start 60 min after injection

After injection, the tracer is cleared from the blood and metabolised in 20 min. ^{18}F-fluoroestradiol binds to the oestrogen receptors on the tumour cell surface as well as intratumoural receptors in oestrogen receptor-positive tumours (Liao et al. 2016).

2019-European Journal of Hybrid Imaging-Giammarile

PET/CT in Breast Cancer

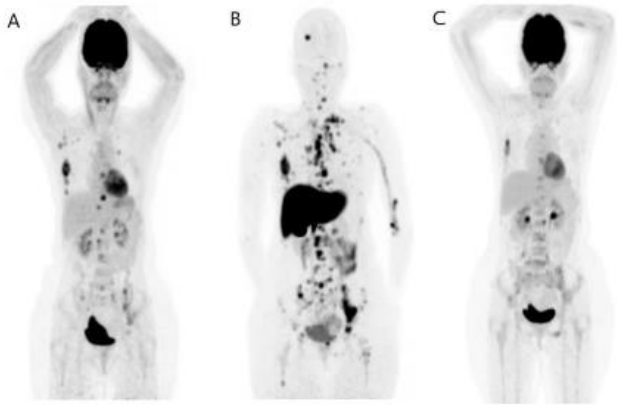

Figure 6. FES PET/CT in treatment guidance. A 50-year-old woman was diagnosed with BR eight years ago and treated with surgery, chemotherapy, and radiotherapy. A recurrence was detected by FDG PET/CT (**A** for MIP image). As the tumor was initially RH+, treatment with fulvestrant was considered. A FES PET/CT was performed prior. Its MIP image (**B**) shows all lesions FDG+ were FES+ and it detected other FDG- lesions. At the evaluation of fulvestrant's treatment response 3 months later, the FDG PET/CT (**C** for MIP image) shows an important partial metabolic response.

2.4. Drawbacks of FDG PET/CT

Various factors can affect the uptake of FDG PET in BC lesions. To be precise, glucose metabolism directly relates to BC aggressiveness. In the same case, the higher ^{18}F-FDG uptake in PET/CT is correlated with undifferentiated histopathology, triple negative receptorial pattern, invasive ductal carcinoma type, and elevated Ki-67 [39]. Similarly, in some conditions with low FDG uptake, there are false-negative PET/CT results. Such conditions include small lesions, low Ki-67 expression, and histology of invasive lobular carcinoma [6,64,65]. Lastly, the factors that may contribute to low PET/CT specificity in patients with high levels of tumor markers include reconstruction artifacts, degenerative bone disease, breast expansion, and lung inflammation [38].

3. FES PET/CT

FES is an analogue of oestradiol fluorinated on the carbon 16 of the D ring (Figure 5). Various fluorinated oestradiol analogues have been proposed during the last three decades for clinical PET imaging. Among them, the FES seems to be the most effective, as it can be produced with a high specific activity and it has a good binding affinity to the oestrogen receptors (ERs) [66–68]. FES uptake depends on both ER density and the availability of ER for ligand binding [69]. Thus, a negative FES PET does not mean there is no malignancy [70].

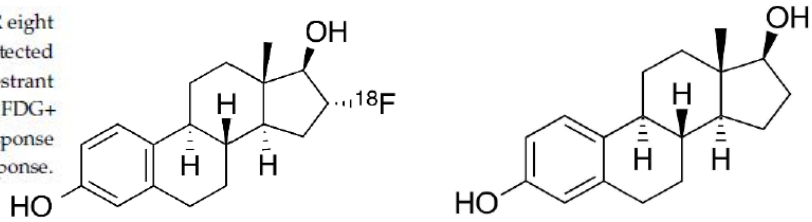

Figure 5. Comparison of chemical structures of FES (left-hand side) and of oestradiol (right-hand side).

2023-J. Clin. Med-yin

^{18}F-fluoroestradiol is a valuable tracer for the studies of the oestrogen receptor status of primary and metastatic breast or ovarian cancers (Venema et al. 2016; van Kruchten et al. 2013a; van Kruchten et al. 2012; van Kruchten et al. 2013b; Peterson et al. 2011; Linden et al. 2011).

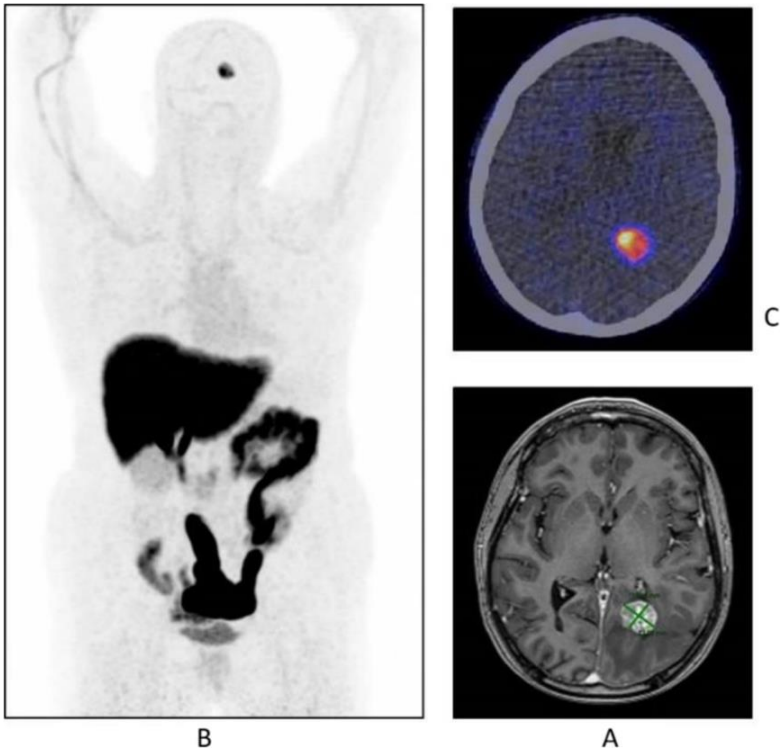

18F-fluoroestradiol, breast cancer, characterisation of brain metastasis. Clinical history: 53 y.o. woman with history of colon cancer (2004) and breast cancer (2011), ER+, presenting with an 18-mm brain lesion on MRI (a).Biopsy was not possible due to location. PET/CT findings: solitary lesion with increased ER expression in the brain in MIP (b), located in the left occipital lobe on fused images (c), suggesting brain metastasis from breast cancer

2019-European Journal of Hybrid Imaging-Giammarile

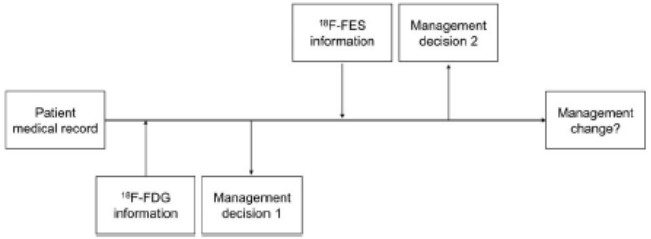

Figure 1. The questionnaire process.
Abbreviations: ^{18}F-FDG, ^{18}F-fluoro-2-deoxy-D-glucose; ^{18}F-FES, 16a-18F-fluoro-17b-estradiol.

Performing 18F-FES PET/CT in newly diagnosed ER-positive breast cancer patients increases the value of diagnosis equivocal lesions and treatment management compared with 18F-FDG PET/CT.

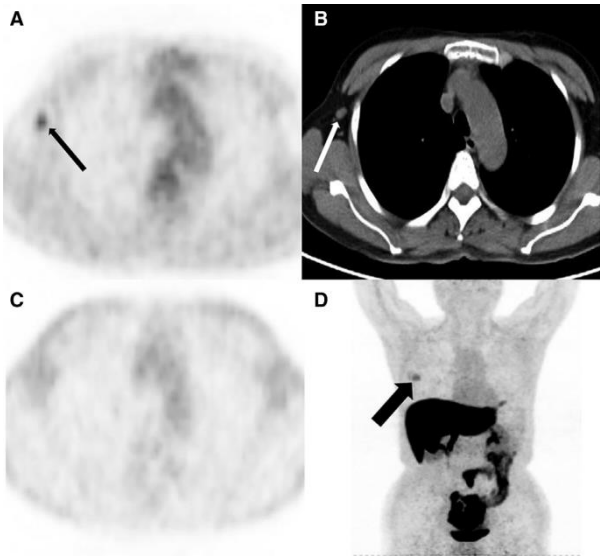

Figure 2. A 49-year-old woman with newly diagnosed estrogen receptor-positive breast cancer. (A): Axial 18F-FDG positron emission tomography (PET) shows right axillary focal uptake (black thin arrow). (B): Axial computed tomography (CT) shows the right axillary lymph node on one level (white thin arrow). (C): At the same level, there is no focal uptake in the 18F-FES PET. (D): 18F-FES PET MIP showed breast mass uptake (black thick arrow) but no focal uptake in right axillary lymph node. The right axillary lymph node was not a metastasis as proven by pathology after operation.

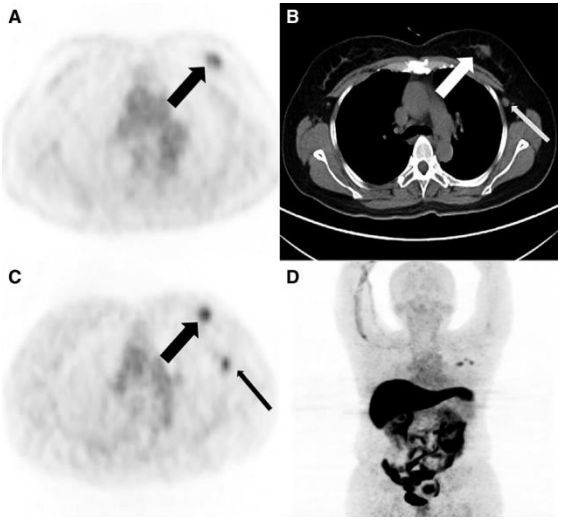

Figure 3. A 54-year-old woman with newly diagnosed ER-positive breast cancer. (A): Axial 18F-FDG positron emission tomography (PET) show left breast mass uptake (black thick arrow). (B): Axial computed tomography (CT) shows a mass at the site of 18F-FDG PET uptake, which is primary breast cancer (white thick arrow) and axillary lymph node (black thin arrow). (C): At the same level, 18F-FES PET shows the mass (black thick arrow) and axillary lymph node (black thin arrow), considered to be estrogen receptor positive lesions. (D): 18F-FES PET MIP demonstrates 18F-FES avid focus in left breast mass and axillary lymph node. The left axillary lymph node contained metastases as proven by pathology after operation.

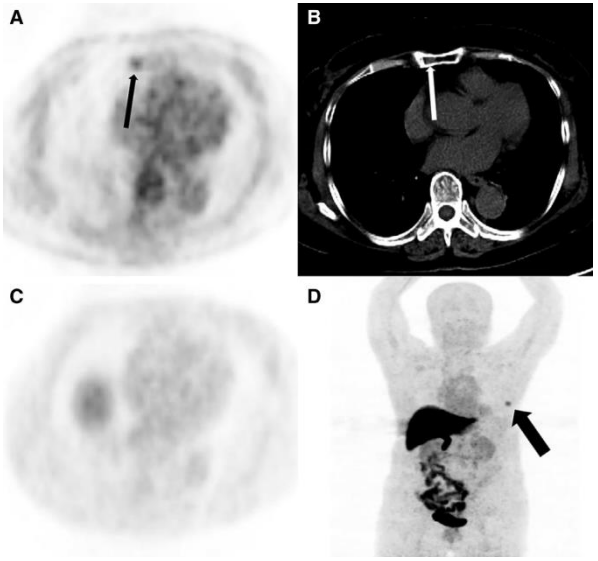

Figure 4. A 71-year-old woman with newly diagnosed estrogen receptor-positive breast cancer. (A): Axial 18F-FDG positron emission
tomography (PET) shows right manubrium focal uptake (black thin arrow). (B): Axial computed tomography (CT) show an inhomogeneous density of partial manubrium on one level (white thin arrow). (C and D): 18F-FES PET has no uptake in the manubrium (black thick arrow shows breast mass uptake). The manubrium lesion was a considered to be a hemangioma during a recent follow-up.

PET imaging in brain

- For cancer diagnostics in general oncology, PET imaging using [18F]-2-fluoro-2-deoxy-d-glucose (FDG) has evolved over the last decades into the most important clinical PET modality.
- Increased glucose metabolism indicated by an increased FDG uptake is commonly seen in proliferating tumors due to the increased glucose transporter expression and the enzyme hexokinase, converting FDG to a phosphorylated product. However, the physiological high FDG uptake in the healthy brain parenchyma hampers the delineation of brain tumors, and cerebral inflammatory processes may also exhibit high FDG uptake, thereby diminishing its diagnostic performance.
- Radiolabeled amino acids are of particular interest for brain tumor imaging using PET because of their increased uptake in neoplastic tissue but low uptake in normal brain parenchyma, resulting in an improved tumor-to-brain contrast.
- Within the group of amino acid PET tracers, [11C]-methyl-l-methionine (MET), 3,4-dihydroxy- 6-[18F]-fluoro-l-phenylalanine (FDOPA), and O-(2-[18F]- fluoroethyl)-l-tyrosine (FET) are frequently used.
- In both gliomas and brain metastases, increased uptake of MET, FET, and FDOPA is related to an increased transport via certain amino acid carriers (amino acid transporters of the L-type (LAT); LAT subtypes 1 and 2), which are overexpressed in neoplastic tissue. Thus, imaging of the amino acid transport in these tumor types using this group of PET tracers is a compelling target.
- In patients with gliomas and brain metastases, a few studies have also used non-FDG and non-amino acid PET imaging. For example, the PET tracer 3'-deoxy-3'-[18F]-fluorothymidine (FLT) is an analog to the nucleoside thymidine and was developed to assess cellular proliferation by tracking the thymidine salvage pathway.

2019-Neuro-Oncology Advances-Galldiks, et al

FET

Names: O-(2-[18F] Fluoroethyl)-L-tyrosine; 18F-fluoroethyltyrosine

^{18}F-FET is an amino-acid PET tracer. After injection, the tracer is trapped into cancerous cells, though it is not incorporated into proteins (Abe et al. 2006).

Diagnosis of central nervous system tumours (very low background in healthy brain) (Galldiks et al. 2015; Albert et al. 2016; Unterrainer et al. 2016; Kunz et al. 2011; Poulsen et al. 2017).

- Fasting for at least 4 h is required
- 4–5 MBq\Kg of ^{18}F-FET iv
- Dynamic one bed brain acquisition for 40 min or static one bed brain acquisitions at 10 and 40–50 min. after injection, for 10 min.

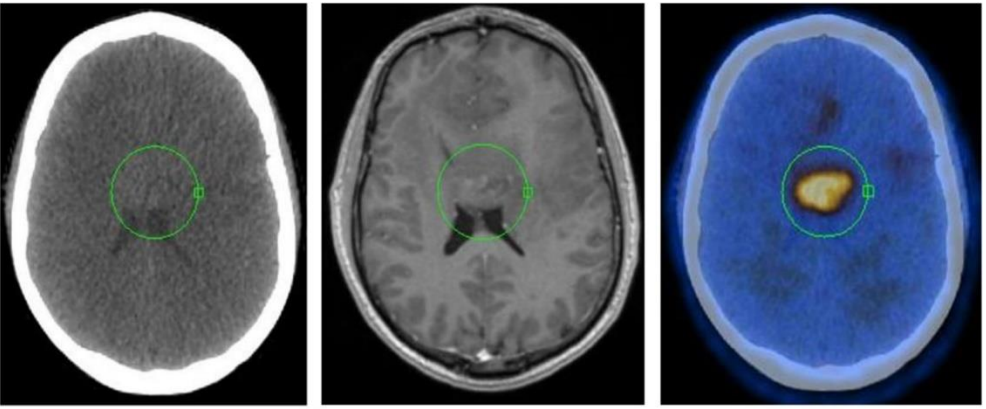

A B C

18F-FET, evaluation of a brain lesion. Clinical history: 46 y.o. man with nausea and headache. CT was non-informative (a). MRI shows an infiltrating lesion with low Gd enhancement (b). PET/CT findings: high FET uptake (c). Surgery confirmed a high-grade glioma

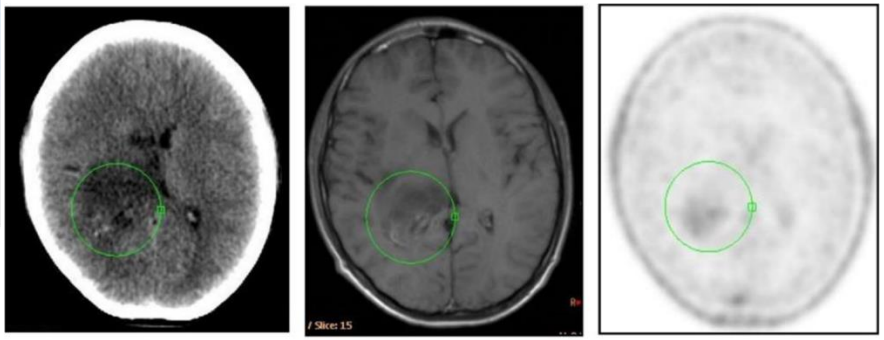

A B C

18F-FET, evaluation of a brain lesion. Clinical history: 46 y.o. man with seizure. CT (a) and MRI (b) shows an infiltrating lesion in the right parietal region (a). PET/CT findings: faint FET uptake in PET (c). Surgery confirmed a low-grade glioma

2019-European Journal of Hybrid Imaging-Giammarile

FLT

Names: 3’-deoxy-3’-[18F]-fluorothymidine; 18F-fluorothymidine

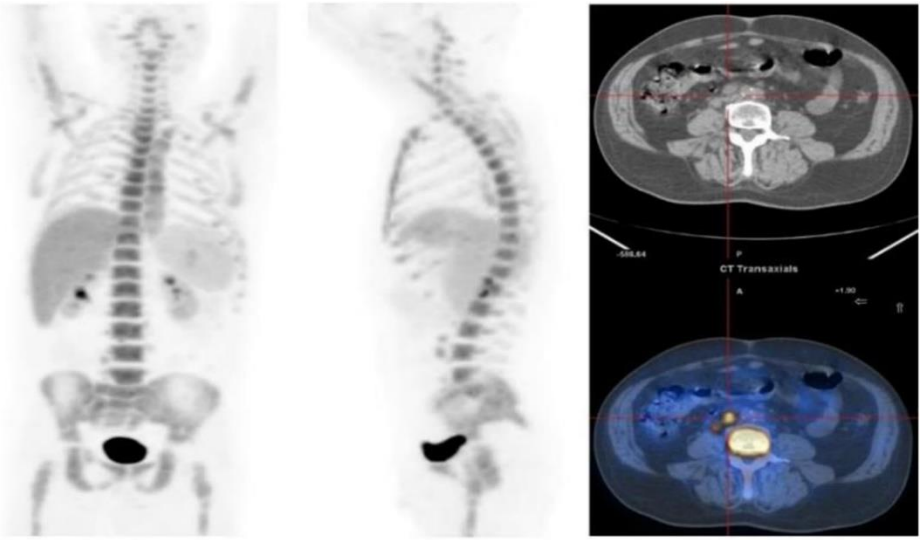

- No fasting is required
- 2–3 MBq\Kg of ^{18}F-FLT iv
- Uptake time 50–60 min

18F-FLT, Hodgkin lymphoma, response evaluation. Clinical history: 32 y.o. patient with Hodgkin lymphoma after second-line therapy. PET/CT findings: moderate uptake of the tracer in two retroperitoneal lymph nodes. a MIP. b MIP in a sagittal view. c CT and fused images

^{18}F-FLT is an analogue of the nucleoside thymidine; however, substitution of the 3′-F atom prevents from further entering the regular biochemical pathway. FLT is transported from the blood into cells by active transport and phosphorylated by thymidine kinase I without incorporation into the DNA. The conjugated FLT is cleared via the kidneys and excreted in the urine. The accumulated activity in the cells is proportional to thymidine kinase 1 activity as well as cellular proliferation (Grierson and Shields 2000; Oh et al. 2004; Shankar 2012; Turcotte et al. 2007; Vesselle et al. 2003).

2019-European Journal of Hybrid Imaging-Giammarile

F-DOPA

Names: L-3,4-Dihydroxy-6-[18F] fluorophenylalanine, 18F-DOPA, 18F-Fluoro-L-DOPA

^{18}F-DOPA reflects all stages of DOPA transport, storage, and metabolism. The tracer is metabolised in the striatum, but also in peripheral tissues such as liver, kidneys, and lung (Rahbar et al. 2017).

Scan acquisition

- Fasting for more than 4 h
- 2–3 MBq/Kg of ^{18}F-DOPA iv
- Uptake time 60 min for extra-cranial tumours. An additional acquisition of 10 min after injection is suggested in medullary thyroid cancer.

- Uptake time 10 min for primary brain tumours.

Clinical indications in oncology (Fig. 39, 40, 41, 42, and 43)

^{18}F-DOPA is used in the detection of neuroendocrine tumours. It is the PET tracer of choice for recurrence detection in patients with medullary thyroid cancer and may play a role in the management of patients with pheochromocytoma and neuroblastoma. ^{18}F-DOPA PET/CT is also used in recurrent glioma (Kratochwil et al. 2017; Chondrogiannis et al. 2013; Soussan et al. 2012; Amodru et al. 2018).

2019-European Journal of Hybrid Imaging-Giammarile

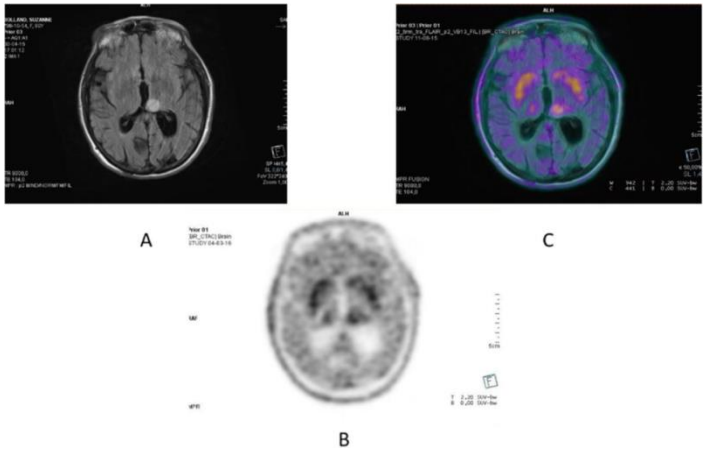

18F-FDOPA, glioma. Clinical history: 61 y.o. woman with indeterminate left thalamic lesion. MRI consistent with low grade glioma (a). PET/CT findings: mild 18F-FDOPA uptake in the lesion, also consistent with low grade glioma (b PET, c fused PET and MR). Follow-up (2 years): no evolution

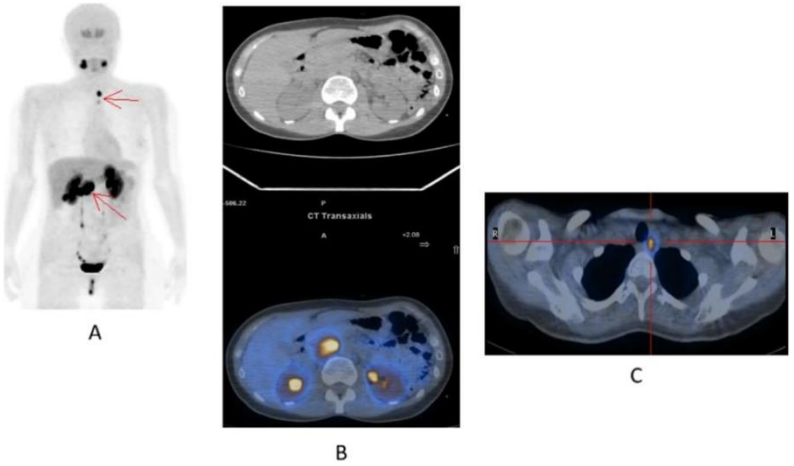

18F-FDOPA, paraganglioma. Clinical history: 48 y.o. man with suspected abdominal paraganglioma. PET/CT findings: intense uptake of the tracer in the abdominal paraganglioma and in a left paratracheal lesion showed in MIP (a), CT and fused images (b and c). Surgery confirmed two paraganglioma lesions

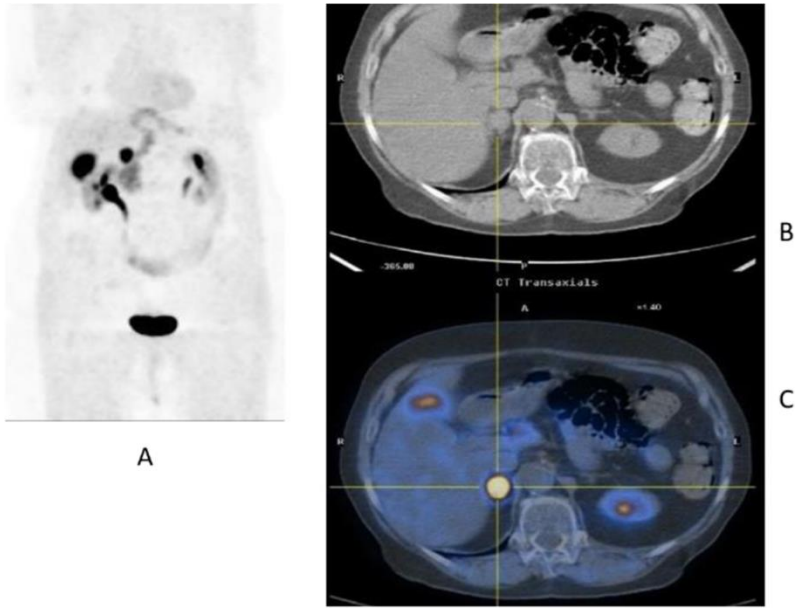

18F-FDOPA, pheochromocytoma. Clinical history: 45 y.o. man with resistant hypertension. Clinical suspicion of phaeochromocytoma. PET/CT findings: intense uptake of the tracer in the right adrenal gland in MIP (a), which is enlarged on CT (b) and fused images (c). Surgery confirmed presence of phaeochromocytoma

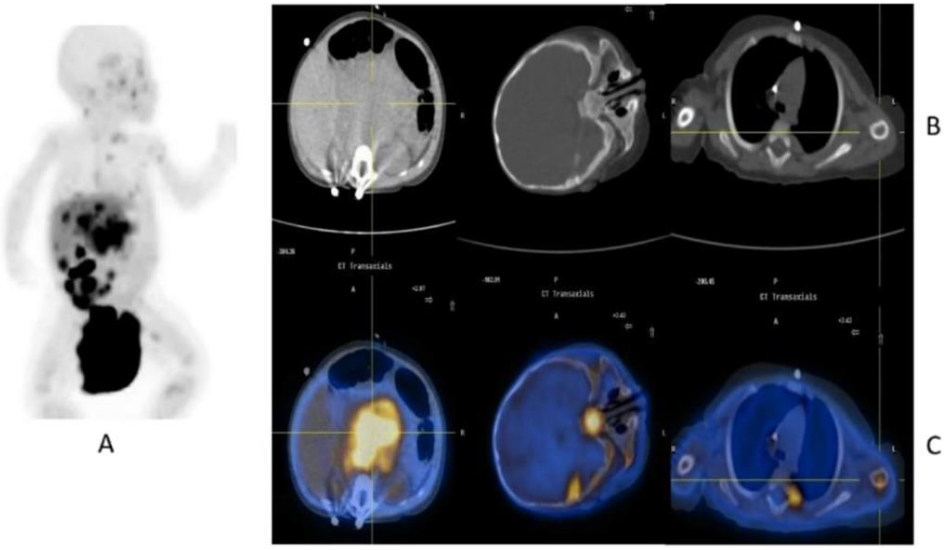

18F-FDOPA, neuroblastoma. Clinical history: 6 months old girl with neuroblastoma, stage IV at presentation. PET/CT findings: intense uptake of the tracer in multiple metastases in the liver and bones, in particular sphenoid and left humerus, seen on MIP (a), CT (b), and fused images (c)

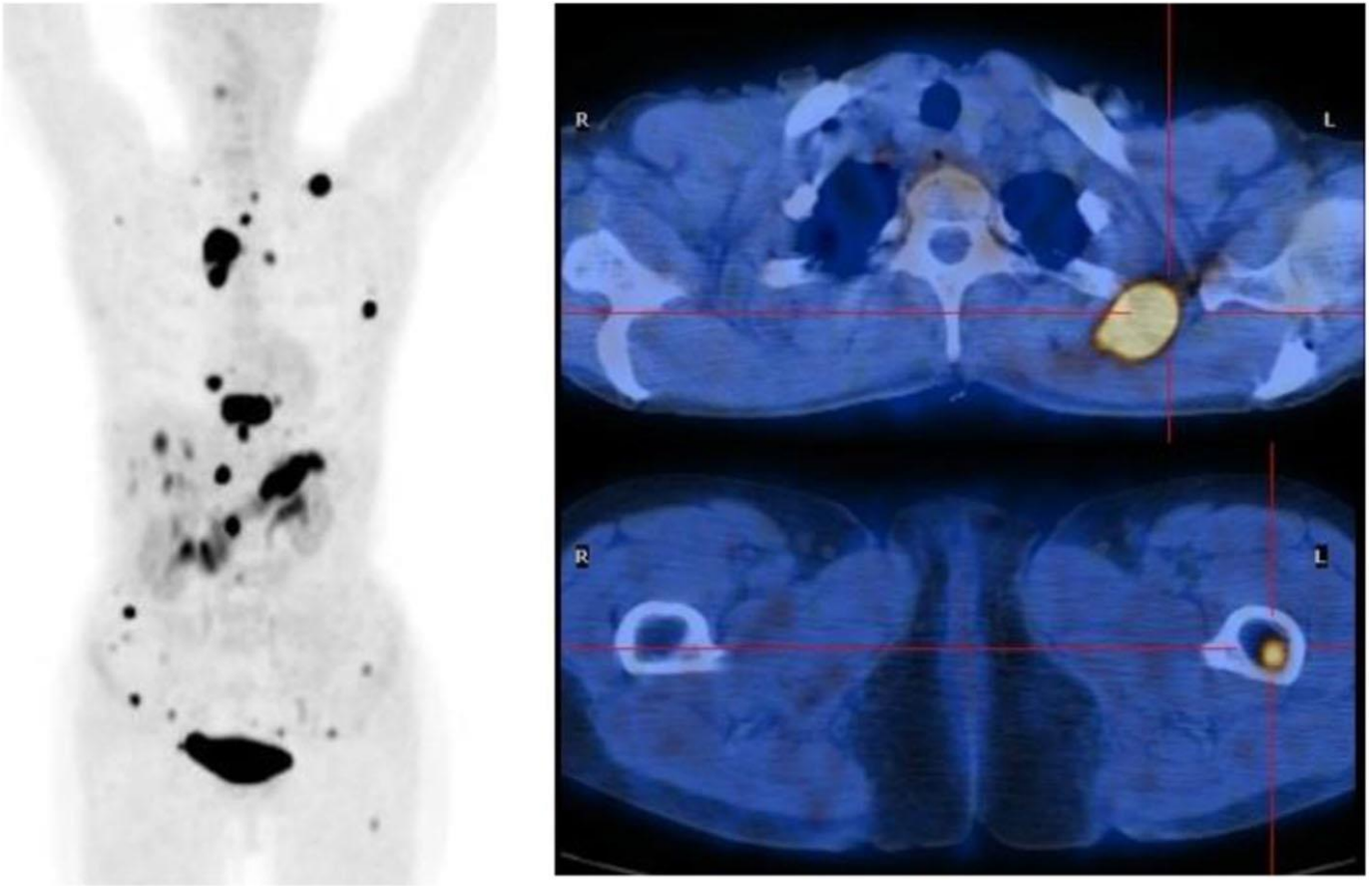

A B

18F-FDOPA, carcinoid. Clinical history: 45 y.o. man with suspected right lung carcinoid. PET/CT findings: intense tracer uptake in the right lung and in multiple bone and soft tissue lesions seen on MIP (a) and fused images (b)

FMISO

Names: 1-(2-Nitro-imidazolyl)-3-[18F] fluoro-2-propanol; 18F-FMISO

Nitro-group are postulated to undergo reduction in hypoxic condition (pO2 ≤ 2–3 mmHg), forming highly reactive oxygen radicals that subsequently bind covalently to macromolecules inside the cells (Visser et al. 2014; Orlefors et al. 2005).

^{18}F-FMISO is relatively hydrophilic and diffuses across cell membranes, showing a passive distribution in normal tissues, resulting in slow clearance kinetics and a high lipophilicity, resulting in substantially high background.

Scan acquisition

- Fasting for at least 2 h
- 6 MBq\Kg of ^{18}F-FMISO iv
- Uptake time 3–4 h

Clinical indications in oncology (Fig. 67)

PET-CT with ^{18}F-FMISO is a non-invasive method for detecting and characterising hypoxia in several tumours. Ischemia in tumours is associated with a poor prognosis, increased invasion rate, metastasis, and resistance to chemo- and radiation therapy (Institute NC 2013; Nehmeh et al. 2008; Gagel et al. 2006; Hirata et al. 2012; Lin et al. 2008; Lopci et al. 2014; Reischl et al. 2007; Wack et al. 2015).

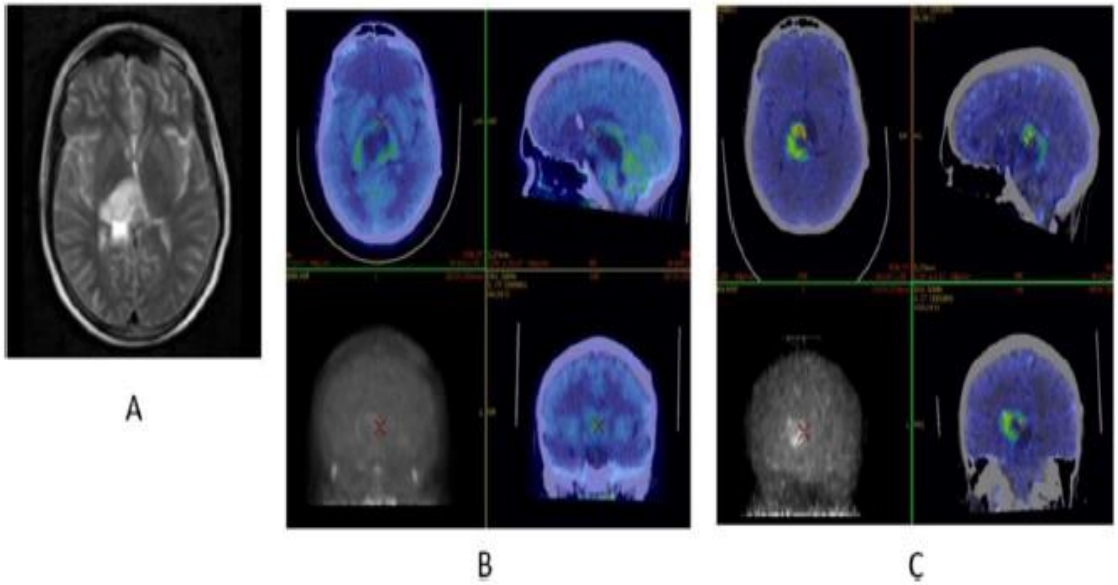

Fig. 67 ^{18}F-FMISO, characterisation of a brain lesion and comparison to ^{11}C-methionine. *Clinical history*: 15 y.o. boy. High-grade glioblastoma, sub-totally removed and treated with radiotherapy. MRI: persistence of expansive lesion in thalamic area (**a**). *PET/CT findings*: ^{11}C-methionine shows peripheral uptake in the right thalamus tumour, probably related to residual viable tumour or relapse despite its low intensity (**b**). ^{18}F-FMISO PET/CT showed hypoxic area in previously methionine uptake described lesion (**c**), suggesting a relapse

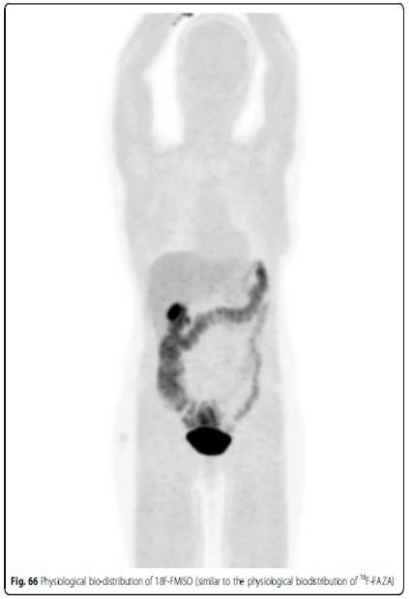

Fig. 66 Physiological bio-distribution of 18F-FMISO (similar to the physiological biodistribution of ^{18}F-FAZA)

Biodistribution and metabolism (Fig. 66)

2019-European Journal of Hybrid Imaging-Giammarile

FAZA

Names: 1-(5-[^{18}F] Fluoro-5-deoxy-α-D-arabinofuranosyl)-2-Nitroimidazole; ^{18}F-FAZA

Biodistribution and metabolism (Fig. 66)

F-18 FAZA is a 2-nitroimidazole compound (reduced in hypoxic cellular media) with a sugar addition moiety showing more water solubility and better pharmacokinetics compared to ^{18}F-FMISO (Zips et al. 2012; Bollineni et al. 2013; Bollineni et al. 2014).

Scan acquisition

- No special diet is required
- 370 MBq of ^{18}F-FAZA iv
- Uptake time 2 h

Clinical indications in oncology (Fig. 68)

The indications are similar to ^{18}F-FMISO (Reischl et al. 2007; Wack et al. 2015; Zips et al. 2012).

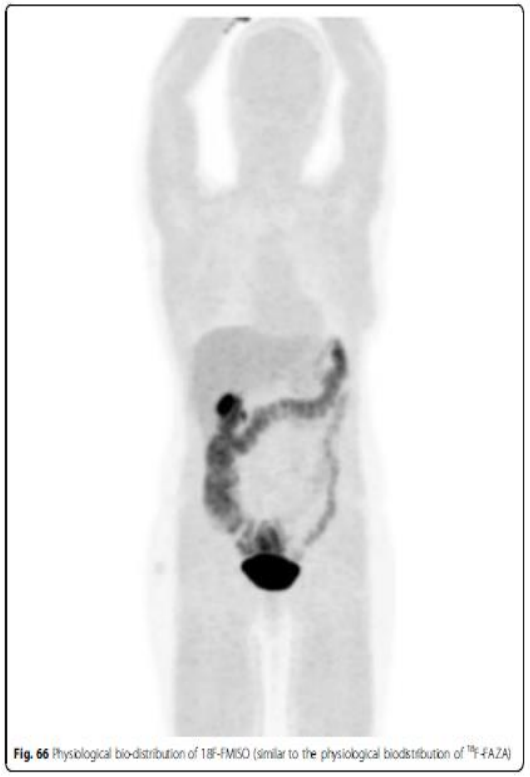

Fig. 66 Physiological bio-distribution of 18F-FMISO (similar to the physiological biodistribution of ^{18}F-FAZA)

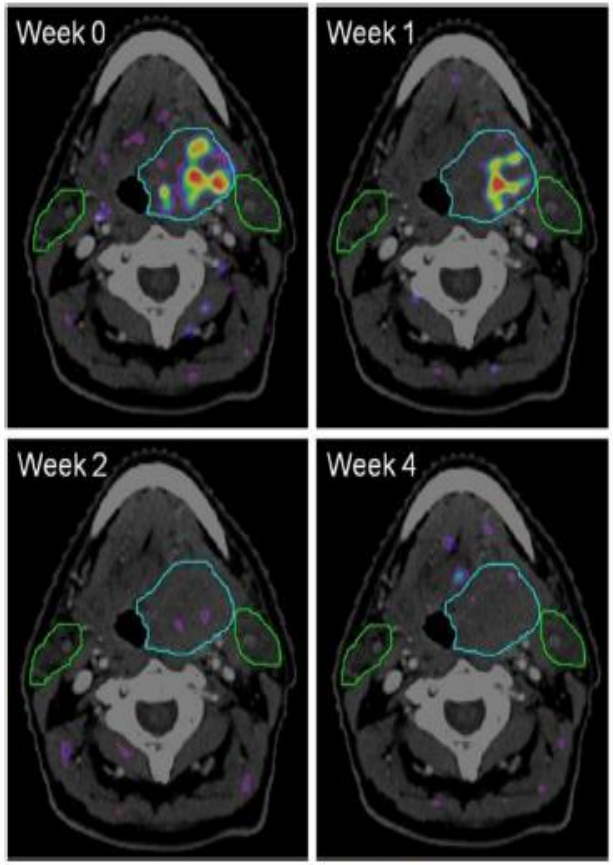

Fig. 68 ^{18}F-FAZA, therapy evaluation of a brain lesion. *PET/CT findings*: four FAZA-PET-CT scans made at different weeks prior (week 0) and during (week 1, 2, and 4) the course of chemoradiation. The rainbow colours depict the amount of FAZA uptake. The light blue line depicts the extent of the primary tumour situated in the base of tongue. The green lines depict the extent of the parotid glands (left and right). Note that in week 2 and 4 no increased FAZA uptake is visible any more, demonstrating that the hypoxic area in week 0 and 1 disappeared

2019-European Journal of Hybrid Imaging-Giammarile

PET imaging in brain

Table 1. Summary of Recommendations

	Gliomas	Meningiomas	Brain metastases
Identification of neoplastic tissue including the delineation of tumor extent	AA PET ++	SSTR PET ++ AA PET + FDG PET –	MRI method of choice AA PET + FDG PET –
Assessment of treatment response	AA PET ++ FLT +	AA PET (++) SSTR PET n.a.	AA PET (++) FLT PET (++)
Differentiation of treatment-related changes from tumor progression at follow-up	AA PET ++	SSTR PET (++)	AA PET ++

++ high diagnostic accuracy; (++) high diagnostic accuracy, but limited data available; + limited diagnostic accuracy; – not helpful; AA PET = amino acid PET; FDG = [^{18}F]-2-fluoro-2-deoxy-D-glucose PET; FLT = 3′-deoxy-3′-[^{18}F]-fluorothymidine PET; n.a. = data not available; SSTR PET = PET using radiolabeled somatostatin receptor ligands.

Key Points

1. In gliomas, radiolabeled amino acids provide important diagnostic information regarding the delineation of tumor extent for treatment planning, diagnosis of treatment-related changes and for the assessment of treatment response.

2. PET ligands for somatostatin receptors may add valuable diagnostic information to standard MRI in meningiomas, especially concerning differential diagnosis and detection of meningioma tissue.

3. Amino acid PET is of great value in distinguishing posttherapeutic reactive changes following radiotherapy from recurrent brain metastases.

2019-Neuro-Oncology Advances-Galldiks, et al

NAF

Names: [^{18}F]-Sodium fluoride; ^{18}F-NaF

Biodistribution and metabolism (Fig. 69)

Fluoride ions are deposited in the bone matrix and reflect: bone remodelling and blood flow. The target organ is bone, but approximately 20% is excreted through the kidney in the urine in the first 1-2 h (Bruine de Bruin et al. 2015; Beheshti et al. 2015).

Scan acquisition

- No special diet is required but good hydration is important
- 50–200 MBq of ^{18}F-NaF iv
- Uptake time 20–60 min

Clinical indications in oncology (Figs. 70 and 71)

The indications are those of 99mTc-labelled diphosphonate bone scintigraphy. ^{18}F-NaF PET/CT is more sensitive than bone scintigraphy, for most indications. The choice of PET or SPECT depends on the availability of the radiopharmaceuticals, PET/CT devices, and costs (Lofgren et al. n.d.).

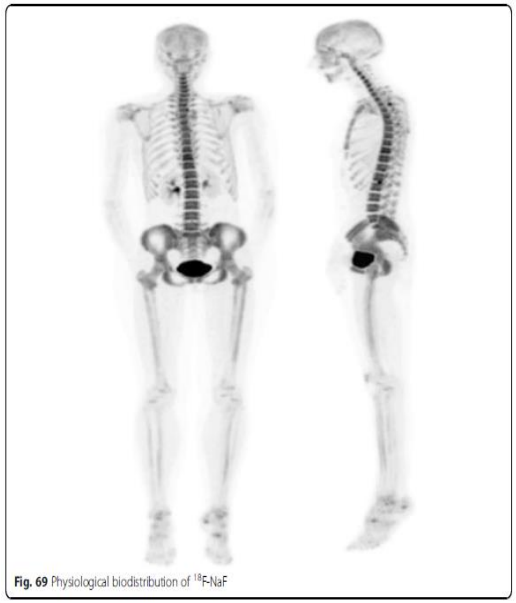

Fig. 69 Physiological biodistribution of ^{18}F-NaF

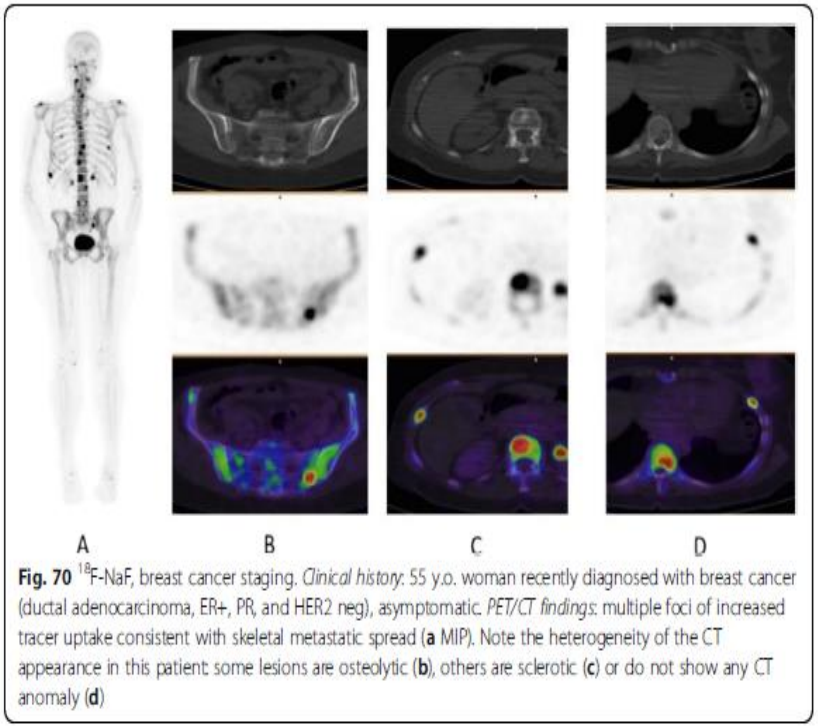

Fig. 70 ^{18}F-NaF, breast cancer staging. *Clinical history*: 55 y.o. woman recently diagnosed with breast cancer (ductal adenocarcinoma, ER+, PR, and HER2 neg), asymptomatic. *PET/CT findings*: multiple foci of increased tracer uptake consistent with skeletal metastatic spread (**a** MIP). Note the heterogeneity of the CT appearance in this patient: some lesions are osteolytic (**b**), others are sclerotic (**c**) or do not show any CT anomaly (**d**)

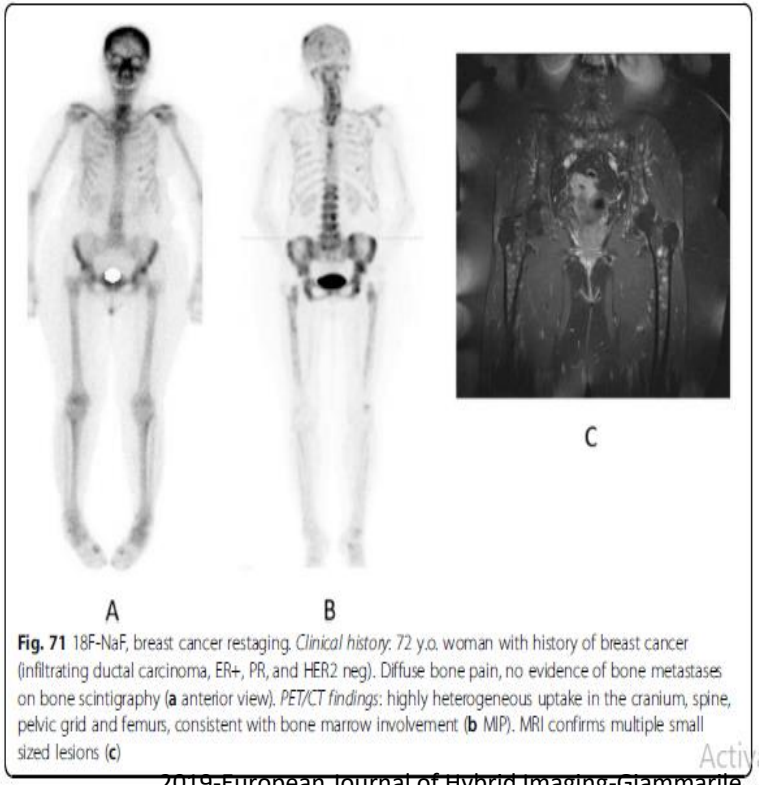

Fig. 71 18F-NaF, breast cancer restaging. *Clinical history*: 72 y.o. woman with history of breast cancer (infiltrating ductal carcinoma, ER+, PR, and HER2 neg). Diffuse bone pain, no evidence of bone metastases on bone scintigraphy (**a** anterior view). *PET/CT findings*: highly heterogeneous uptake in the cranium, spine, pelvic grid and femurs, consistent with bone marrow involvement (**b** MIP). MRI confirms multiple small sized lesions (**c**)

2019-European Journal of Hybrid Imaging-Giammarile

Application of PET Tracers in Breast Cancer

Other PET Tracers for Molecular Imaging in BC

Multiple new tracers of potential interest in BC can be identified (see Table 2). PET imaging of additional receptors may be the next step, for example, the hormone receptor tracer [^{18}F]-dihydrotesterone ([^{18}F]-FDHT)-PET, which is commonly used in prostate cancer trials. This tracer provides information about androgen receptor (AR) expression, which is a potential new target for BC treatment [46]. Moreover, cell proliferation can be detected by [^{18}F]-fluorothymidine ([^{18}F]-FLT)-PET, and post-neoadjuvant chemotherapy [^{18}F]-FLT uptake may be correlated with the proliferation marker Ki-67 measured by IHC in primary BC patients [92]. In light of the current developments in BC immunotherapy, assessment of the programmed death-ligand 1 (PD-L1) with [^{89}Zr]-labeled atezolizumab is clearly of interest. Recently, a first-in-human study with 22 patients (including 4 with triple-negative BC) showed a better correlation of [^{89}Zr]-atezolizumab uptake to treatment response, PFS and OS at patient level than the commonly used SP142 IHC marker [93]. Currently, one recruiting [^{89}Zr]-atezolizumab-PET study is available for lobular BC (*NCT04222426*). Furthermore, a combination of molecular imaging techniques, such as [^{18}F]-FES-PET, [^{89}Zr]-trastuzumab-PET with [^{18}F]-FDG-PET, may be useful in identifying disease heterogeneity or differentiating between indolent and aggressive disease [48, 54, 94]. This could help to select the best therapeutic strategy.

Table 2 Ongoing PET imaging based clinical trials including breast cancer patients ($n = 48$)

Radiotracer	Target	Description of disease characteristics	Estimated enrollment	Phase	Trial ID	(estimated) Study start year	Status
[^{18}F]-FES	ER	ER+, HER2− MBC	60	NA	NCT03442504	2017	Recruiting
		ER+, HER2− MBC	8	I/II	NCT04150731	2020	Not yet recruiting
		ER+ (M)BC	60	III	NCT03544762	2017	Recruiting
		ER+, HER2− MBC	75	II	NCT02409316	2015	Recruiting
		ER+ MBC	68	NA	NCT03768479	2017	Recruiting
		ER+, HER2− MBC	104	I	NCT03455270	2018	Recruiting
		ER+, HER2− locally advanced and locoregional recurrent BC	40	NA	NCT03726931	2018	Recruiting
		ER−, HER2+ MBC	33	NA	NCT03619044	2019	Not yet recruiting
		ER+ MBC	100	NA	NCT04125277	2019	Recruiting
		ER+ MBC	99	II	NCT02398773	2016	Recruiting
		ER+, HER2− MBC	25	NA	NCT03873428	2020	Not yet recruiting
		ER+ (M)BC	100	I	NCT01916122	2013	Recruiting
		ER+ recurrent BC or MBC	100	NA	NCT00816582	2010	Active, not recruiting
		Regardless of ER/HER2 status, MBC	217	NA	NCT01957332	2013	Active, not recruiting
		ER+ (M)BC	29	NA	NCT02149173	2010	Active, not recruiting
		ER+, HER2− MBC	16	I	NCT02650817	2016	Active, not recruiting
		ER+ MBC	15	NA	NCT01720602	2012	Active, not recruiting
[^{18}F]-FDHT	AR	AR+, HER2− MBC	22	II	NCT02697032	2016	Active, not recruiting
[^{18}F]-FTT	PARP-1	(M)BC	30	NA	NCT03846167	2019	Recruiting
		BC	30	I	NCT03083288	2017	Active, not recruiting
[^{18}F]-ISO-1	Sigma-2 receptor	MBC	30	NA	NCT03057743	2016	Recruiting
		BC	30	I	NCT02284919	2014	Active, not recruiting
[^{18}F]-FLT	Thymidine kinase activity	Regardless of ER/HER2 status, Rb + MBC	20	I	NCT02608216	2015	Recruiting
		MBC	17	NA	NCT01621906	2012	Active, not recruiting
[^{18}F]-FMISO	Hypoxic cells	ER−, HER2− MBC	126	II	NCT02498613	2016	Recruiting
[^{18}F]-GE-226	HER2	MBC	16	NA	NCT03827317	2019	Recruiting
[^{18}F]-F-GLN	Glutamine metabolism	(M)BC	30	NA	NCT03863457	2019	Recruiting
[^{18}F]-$\alpha_v\beta_6$-BP	$\alpha_v\beta_6$	(M)BC	27	I	NCT03164486	2016	Recruiting
[^{18}F]-Var3	Extracellular pH	MBC	10	I	NCT04054986	2019	Recruiting
[^{18}F]-Flutemetamol	Amyloid beta	BC	15	NA	NCT02317783	2015	Recruiting
[^{18}F]-FSPG	Amino acid transporter x_c^-	BC	120	NA	NCT03144622	2016	Recruiting
[^{18}F]-FAZA	Hypoxic cells	BC	25	I	NCT03168737	2017	Recruiting
[^{18}F]-ASIS	Tissue factor	(M)BC	10	I	NCT03790423	2019	Recruiting
[^{89}Zr]-Trastuzumab	HER2	Regardless of ER/HER2 status, MBC	217	NA	NCT01957332	2013	Active, not recruiting
[^{89}Zr]-Atezolizumab	PD-L1	ER−, HER2− MBC	54	NA	NCT02453984	2016	Recruiting

2020-Current Oncology Reports-Boers

Application of PET Tracers in Breast Cancer

Zr89

Zr-89 can be produced by bombarding stable yttrium-89 (Y-89) with protons in a cyclotron. The reaction can be represented as follows:

$^{89}Y(p,n)^{89}Zr$

• This method involves using a cyclotron to accelerate protons, which are then directed at a target containing Y-89.

In some cases, Zr-89 is obtained from a strontium-82 (Sr-82) generator system, where Sr-82 decays to Zr-89. However, this is more commonly associated with Rb-82 production

Molecular imaging in breast cancer (BC) is of particular interest, as it can visualize the estrogen receptor (ER), human epidermal growth factor receptor 2 (HER2), and proliferation.

Trastuzumab is a type of targeted cancer drug called a monoclonal antibody

Development Stages of [^{89}Zr] -Trastuzumab-PET/CT

Technical Validity

The [^{89}Zr]-labeled antibody trastuzumab binds to the HER2-receptor and has a relatively long half-life (t ½ = 78 h). This enables imaging at late time points but also limits repeatability testing as radiation dose is high and repeated scans would require a 2-week interval [86]. To optimize the acquisition protocol, imaging at multiple time points (after 1–7 days) was performed after a single tracer injection [87, 88]. The optimal time point was found after 4–5 days, due to lower background uptake and higher contrast. Recently, a [^{89}Zr]-PET/CT EARL accreditation program was established, similar to [^{18}F]-FDG-PET/CT accreditation [60, 89, 90••].

2020-Current Oncology Reports-Boers

89Zr-Pertuzumab PET/CT

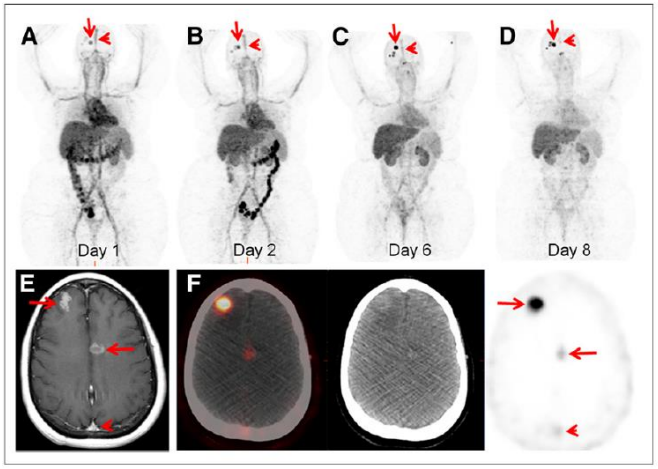

FIGURE 3. 46-y-old woman with both HER2-positive and HER2-negative primary breast malignancies and recently diagnosed brain metastases. Sequential maximum-intensity-projection images 1 d (A), 2 d (B), 6 d (C), and 8 d (D) after administration of ^{89}Zr-pertuzumab. Blood-pool and liver background cleared on sequential images. Activity excreted by bowel was seen on days 1 and 2. Bilateral kidney activity was visualized on all days. Increasing activity in foci overlying skull was seen as time progressed (arrows). Decreasing activity was seen in blood pool of superior sagittal sinus (arrowheads). (E) Gadolinium-enhanced T1-weighed MR image of brain demonstrated enhancing brain metastases (arrows) and superior sagittal sinus (arrowhead). (F) Axial fused PET/CT, CT, and PET images 8 d after ^{89}Zr-pertuzumab administration demonstrated avidity in brain metastases (arrows) and minimal residual avidity in superior sagittal sinus (arrowhead).

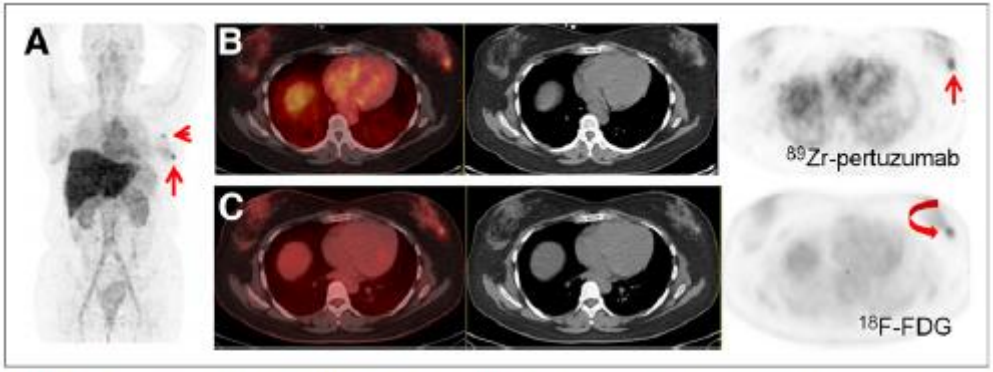

FIGURE 4. 58-y-old woman with HER2-positive breast cancer and current left breast and left axillary nodal disease. (A) Maximum-intensity-projection image 6 d after administration of ^{89}Zr-pertuzumab demonstrated ^{89}Zr-pertuzumab–avid left breast (arrow) and left axillary nodal (arrowhead) disease. (B) Axial fused PET/CT, CT, and PET images obtained 6 d after ^{89}Zr-pertuzumab administration localized ^{89}Zr-pertuzumab avidity in left breast (arrow). (C) Axial fused PET/CT, CT, and PET images from ^{18}F-FDG PET/CT scan 3 wk earlier demonstrated corresponding ^{18}F-FDG–avid breast lesion (arrow).

Human epidermal growth factor receptor 2 (HER2) is a critical biomarker in breast cancer, and its expression directly influences treatment. Approximately 20% of invasive ductal breast malignancies are classified as HER2-positive as a result of ERBB2 gene amplification or the subsequent overexpression of the HER2 protein on the surface of tumor cells (1). Patients with HER2-positive breast cancer receive specific therapies that are targeted to HER2 and that reduce the risk of death, whereas patients with HER2-negative breast cancer do not receive them (2,3). This situation has resulted in considerable interest in HER2-targeted imaging (4). Recent work has demonstrated the ability to detect HER2-positive metastases in patients with HER2-negative primary breast tumors by HER2-targeted imaging confirmed with immunohistochemistry (IHC) (5,6) and molecular analyses (7). Thus, the ability to perform noninvasive, whole-body, HER2-targeted imaging may be valuable in the detection of otherwise unsuspected HER2-positive malignancies and may help direct appropriate HER2-targeted therapy. Pertuzumab is a newer humanized monoclonal antibody that binds to the HER2 receptor at a site distinct from that bound to by trastuzumab and appears to be more efficient than trastuzumab (8). In vitro and in vivo models have demonstrated successful 89Zr-pertuzumab targeting to HER2-positive malignancies and, notably, have demonstrated increased affinity for HER2 in the presence of trastuzumab (9)—as may be the case in patients who have HER2-positive malignancies and are receiving trastuzumab.

2018-J Nucl Med-Ulaner

Application of PET Tracers in Breast Cancer

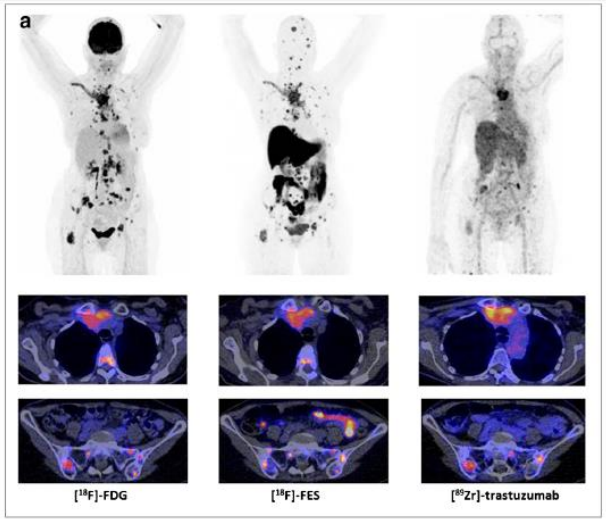

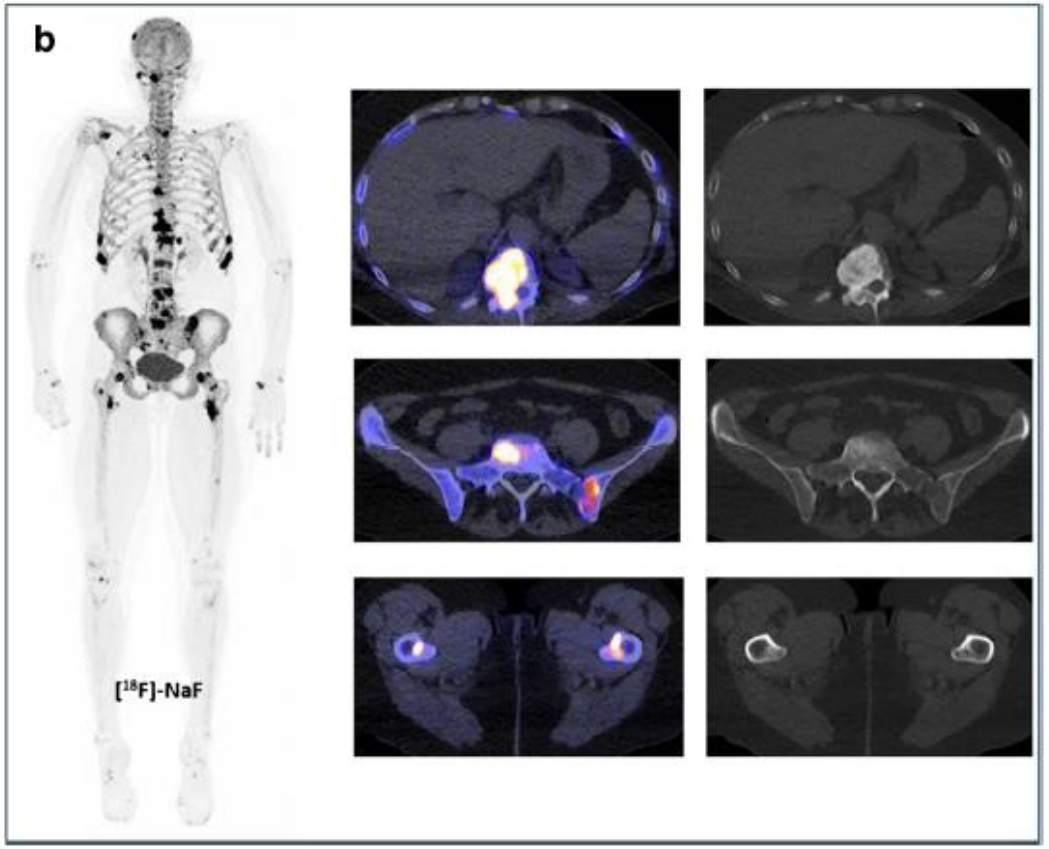

Fig. 1 Upper image: three PET scans ([^{18}F]-FDG-PET, [^{18}F]-FES-PET, and [^{89}Zr]-trastuzumab-PET) in the same patient showing mediastinal and hilar lymph node metastases, as well as intrapulmonary lesions visible on both [^{18}F]-FDG-PET and [^{18}F]-FES-PET, but not on [^{89}Zr]-trastuzumab-PET. The large mediastinal mass (first row of transversal fused images) was visible on all three imaging modalities. Bone metastases (second row of transversal fused images) were clearly visualized on [^{18}F]-FES-PET, for example, skull lesions, and to a lesser extent on [^{18}F]-FDG-PET and [^{89}Zr]-trastuzumab-PET. Lower image: [^{18}F]-NaF-PET in another patient showing bone metastases in the skull, vertebrae, costae, pelvis, and proximal femora. The increased uptake in the joint was related to degeneration

2020-Current Oncology Reports-Boers

Ga68

Production Method: cyclotron
Can be Ga-68 can be produced via a generator system from germanium-68:

$^{68}Ge \rightarrow {}^{68}Ga + \beta^-$

1. **Parent Isotope**: The generator typically contains Germanium-68 (Ge-68) as the parent isotope. Ge-68 has a long half-life (about 270 days), allowing the generator to be used over an extended period.

2. **Elution Process**: The Ga-68 is extracted from the generator through an elution process, where a suitable solvent (usually saline) is passed through the generator to wash out the Ga-68. This process can be repeated multiple times, producing Ga-68 for clinical use.

PET imaging in brain

- Owing to the overexpression of somatostatin receptors (SSTR) in meningiomas, radiolabeled SSTR ligands allow the visualization of meningiomas using PET. It has been observed that the SSTR subtype 2 is the most abundant isoform, with approximately 100% expression in meningioma tissue.
- For PET imaging, SSTR ligands are typically labeled with 68Ga (half-life, 68 min).
- The 68Ga-labeled tracers DOTA-D-Phe1-Tyr3-octreotate (DOTATATE) and DOTA-Tyr3-octreotide (DOTATOC) are the most common applied tracers in the clinical management of meningioma patients and can also be used for the imaging of patients with neuroendocrine tumors, which as well express high levels of SSTR. Furthermore, these tracers provide an excellent lesion-to-background contrast, which is related to a low uptake in bony structures and healthy brain parenchyma.

2019-Neuro-Oncology Advances-Galldiks, et al

PET imaging in brain

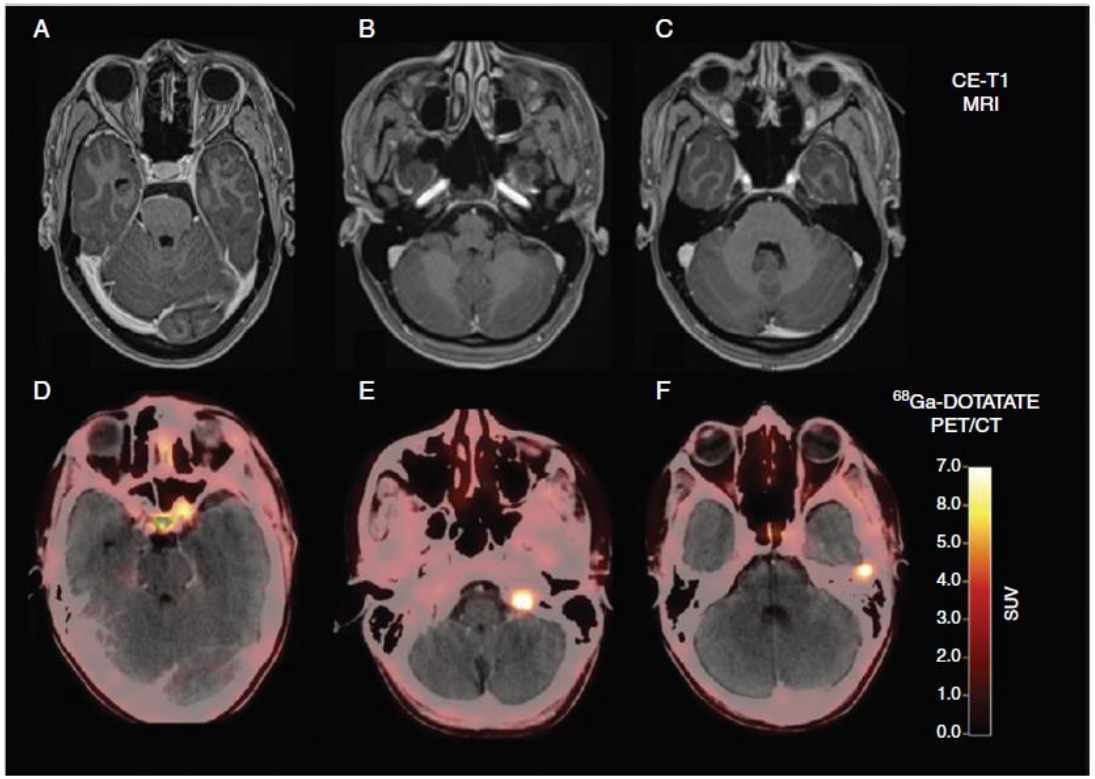

Fig. 2 Postoperative contrast-enhanced MRI and DOTATATE PET/CT of a 32-year-old patient after resection of a World Health Organization grade I meningioma show residual tumor located at the left internal carotid artery and at tumor at the tip of the left orbit (A and D). Surprisingly, 2 additional meningiomas were also visible on the DOTATATE PET/CT (E and F), without corresponding contrast enhancement on MRI (B and, C) (reproduced from Galldiks et al.,[14] with permission from Oxford University Press).

In meningiomas, target volumes are frequently delineated based on coregistered contrast enhanced tomographic images (MRI and CT). However, in meningiomas located at the skull base (approximately onethird of cases), it is difficult to differentiate between meningioma tissue and dura and/or bone, because of a high contrast enhancement of these structures. Moreover, in transosseous meningiomas, it is difficult to exactly define the degree of infiltration, despite using the bone window on CT images. In the setting of the identification of meningioma remnants after incomplete resection (Figure 2), PET imaging seems to be helpful for adjuvant radiotherapy planning.

2019-Neuro-Oncology Advances-Galldiks, et al

68Ga-DOTA Peptides

68Ga-DOTA-Phe1-Tyr3-octreotide (TOC)

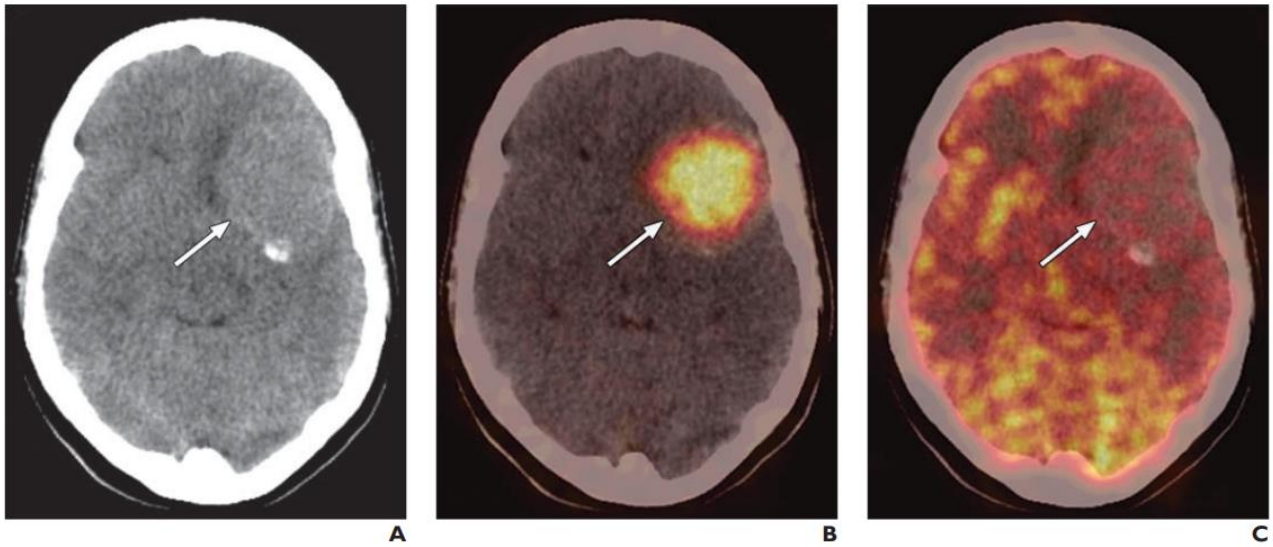

Fig. 1—45-year-old woman with meningioma.
A, Transaxial CT image reveals large extraaxial left frontal space–occupying lesion (*arrow*) with calcification and no significant perilesional edema.
B and **C,** Lesion (*arrow*) shows intense tracer uptake on transaxial ^{68}Ga-labeled tetraazacyclododecanetetraacetic acid–Phe^{1}-Tyr^{3}-octreotide PET/CT image (**B**) but is hypometabolic on transaxial ^{18}F-FDG PET/CT image (**C**). Diagnosis of meningioma was made and confirmed after surgery.

68Ga-DOTA-NaI3-octreotide (NOC),

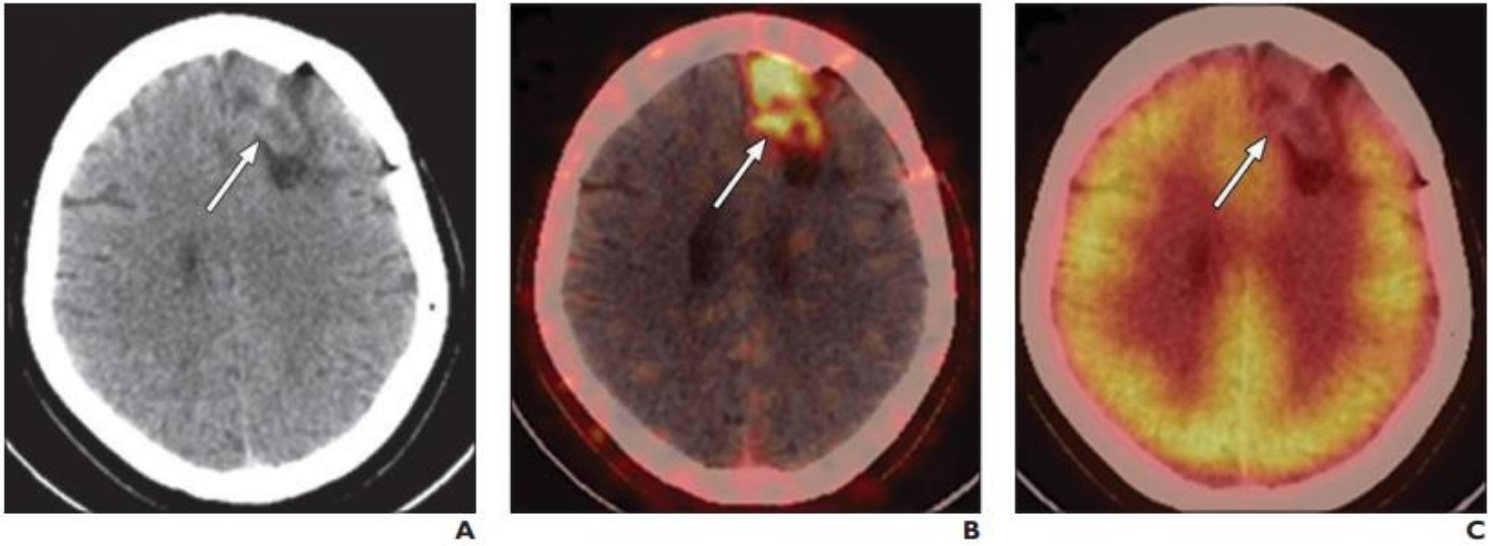

Fig. 3—32-year-old woman with suspected recurrence of meningioma.
A, Transaxial unenhanced CT shows ill-defined isodense-to-hyperdense lesion (*arrow*) in postoperative cavity in left frontal lobe.
B, Increased ^{68}Ga-labeled tetraazacyclododecanetetraacetic acid–NaI^{3}-octreotide uptake is noted in this lesion (*arrow*) on transaxial PET/CT image, suggesting recurrence.
C, However, transaxial ^{18}F-FDG PET/CT image was negative for recurrence (*arrow*). Diagnosis of recurrence meningioma was confirmed at surgery.

2013-Nuclear Medicine and Molecular Imaging-sharma

68Ga-DOTA Peptides

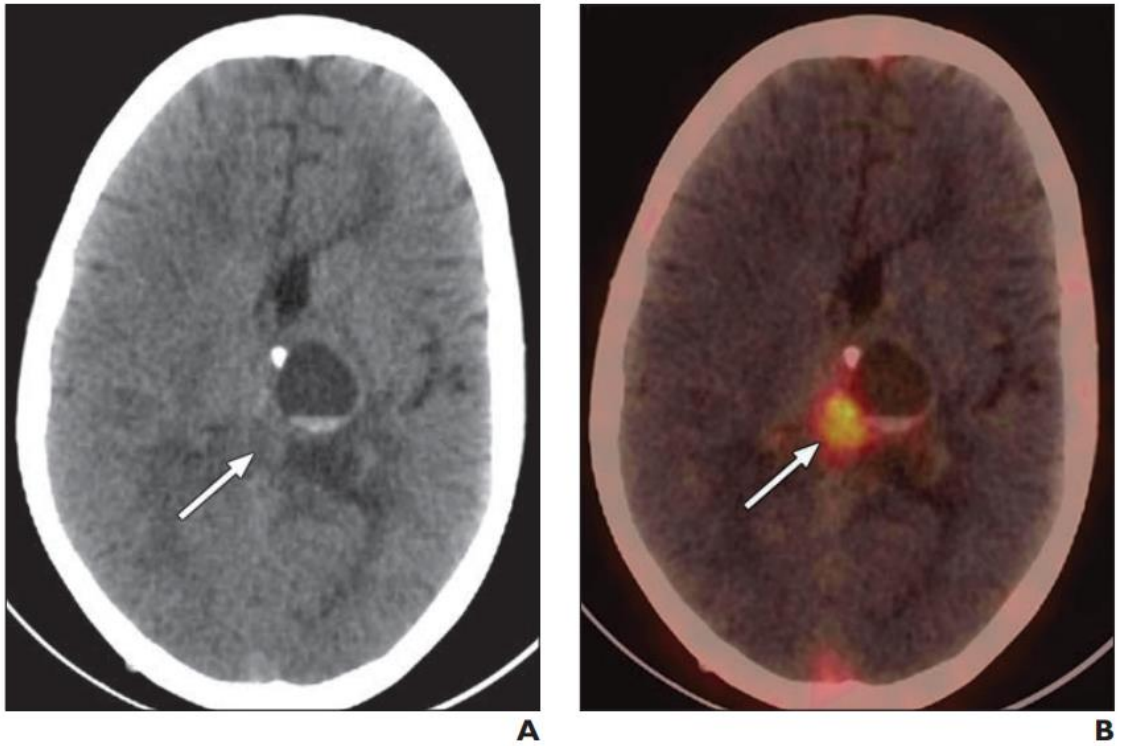

Fig. 6—14-year-old girl with supratentorial primitive neuroectodermal tumor (PNET).
A, Transaxial unenhanced CT image of brain shows solid cystic left thalamic space–occupying lesion (*arrow*) with calcification.
B, Transaxial ^{68}Ga-labeled tetraazacyclododecanetetraacetic acid–NaI^{3}-octreotide PET/CT image of brain shows increased tracer uptake (*arrow*) in solid component of tumor, suggesting diagnosis of supratentorial PNET. Biopsy confirmed diagnosis of supratentorial PNET.

68Ga-DOTA-NaI3-octreotide (NOC),

68Ga-DOTA-Phe1-Tyr3-octreotide (TOC)

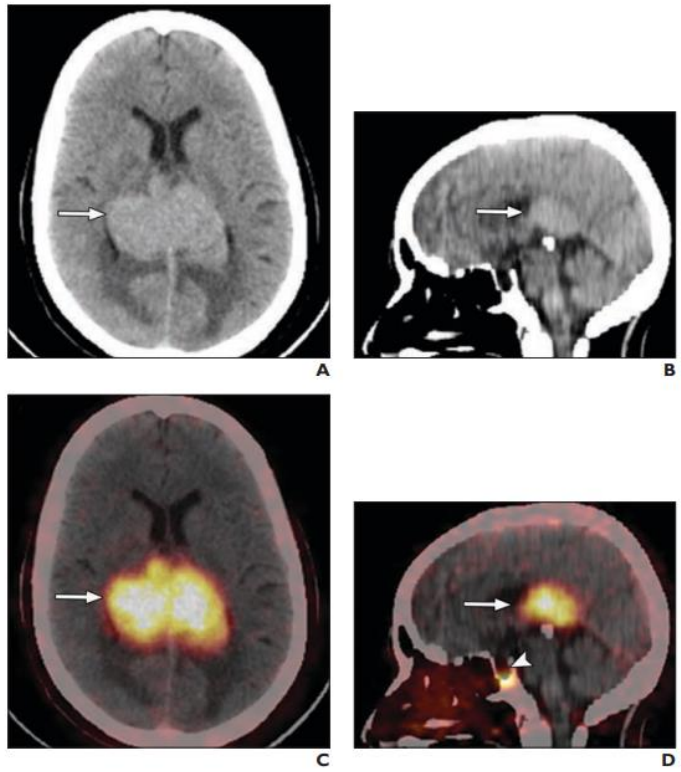

Fig. 2—72-year-old woman with suspected splenial meningioma.
A and **B,** Transaxial (**A**) and sagittal (**B**) unenhanced CT images show large hyperdense parasplenial mass (*arrow*).
C and **D,** Transaxial (**C**) and sagittal (**D**) ^{68}Ga-labeled tetraazacyclododecanetetraacetic acid–Phe^{1}-Tyr^{3}-octreotide PET/CT images reveal intense tracer uptake in parasplenial mass (*arrow*), confirming diagnosis. Also note physiologic pituitary uptake (*arrowhead*, **D**).

2013-Nuclear Medicine and Molecular Imaging-sharma

Advances in PET imaging for meningioma and Neuroendocrine tumors

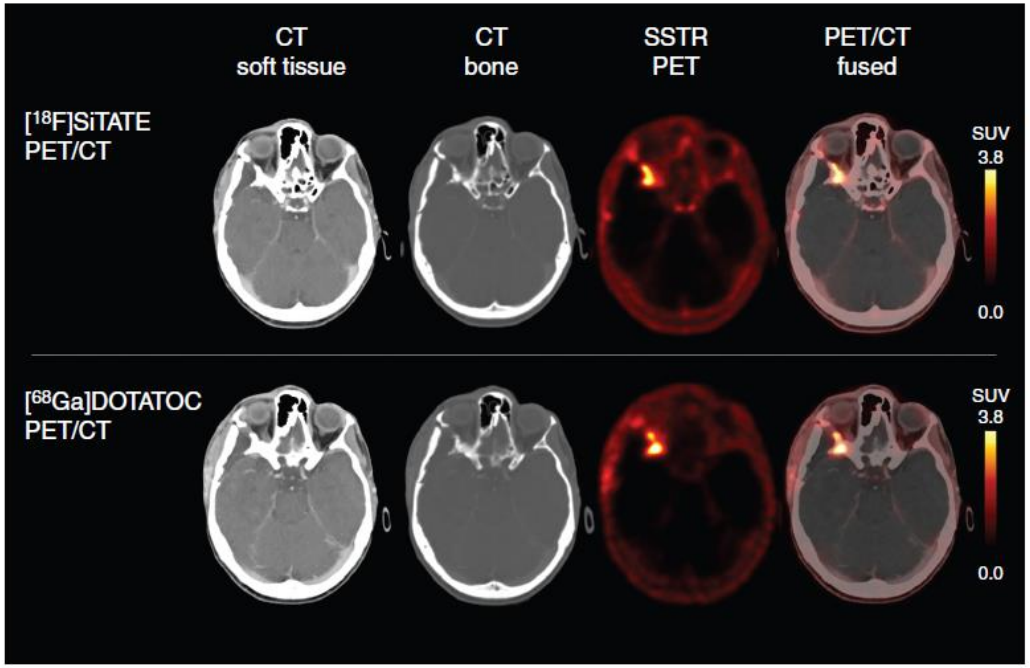

Figure 1. ^{18}F-SiTATE (top row) and ^{68}Ga-DOTATATE PET/CT (bottom row) of a patient after resection of a WHO grade I sphenoid wing meningioma show residual tumor laterally located to the right orbit. Visually, tumoral uptake on ^{18}F-SiTATE was highly comparable to ^{68}Ga-DOTATATE PET/CT. Note the lower spatial resolution of the ^{68}Ga-labeled peptide DOTATATE compared to ^{18}F-SiTATE PET.

The tracer 18F-SiTATE (also known as 18F-SiFAlin-TATE) is a novel 18F-labeled SSTR targeting peptide providing high tumor uptake, excellent image quality, and economic and logistic advantages of 18F- over 68Ga-labeled compounds. In particular, a cost-intensive 68Ge/68Ga generator is no longer necessary for tracer radiosynthesis. Furthermore, the labeling approach of 18F-SiTATE is straightforward and automated. An initial report in a meningioma patient suggested that tumor delineation of 18F-SiTATE PET is equivalent to 68Ga-DOTATOC PET but with higher resolution. A similar example is presented in Figure 1. Further studies in meningioma patients using 18F-SiTATE PET imaging are warranted.

[^{18}F]SiTATE (formerly known as [^{18}F]SiFA*lin*-TATE) was recently introduced as a highly promising imaging agent for the diagnosis of well-differentiated Neuroendocrine tumors (NET) using positron emission tomography/computed tomography (PET/CT). A high tumor uptake and excellent image quality, the straightforward labeling approach, as well as the economic and logistic advantages of ^{18}F- over ^{68}Ga-labeled compounds predestinate [^{18}F]SiTATE to become a potential new clinical reference standard.

2023-Neuro-Oncology Advances-Galldiks et al

18F-FDG PET/CT & 68Ga-DOTATATE PET/CT

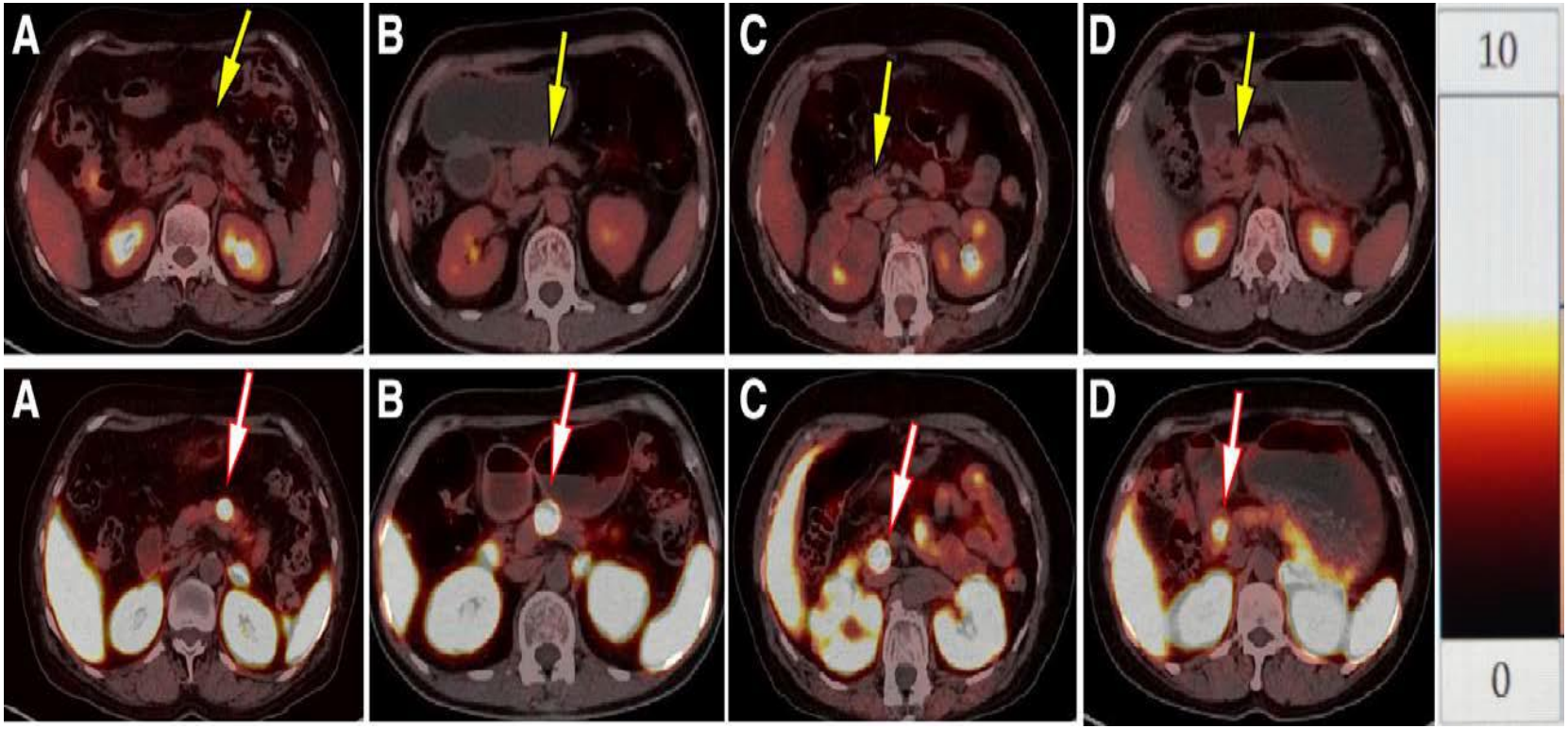

A–D) 18F-FDG PET/CT fusion images of 4 false negative G1 grade NET cases; (A–D) the corresponding 68Ga-DOTATATE PET/CT fusion images showed significant radioactive uptake of the lesions, CT = computed tomography, NET = neuroendocrine tumors, PET = positron emission tomography.

2023-medicine-Xianwen

18F-FDG PET/CT & 68Ga-DOTATATE PET/CT

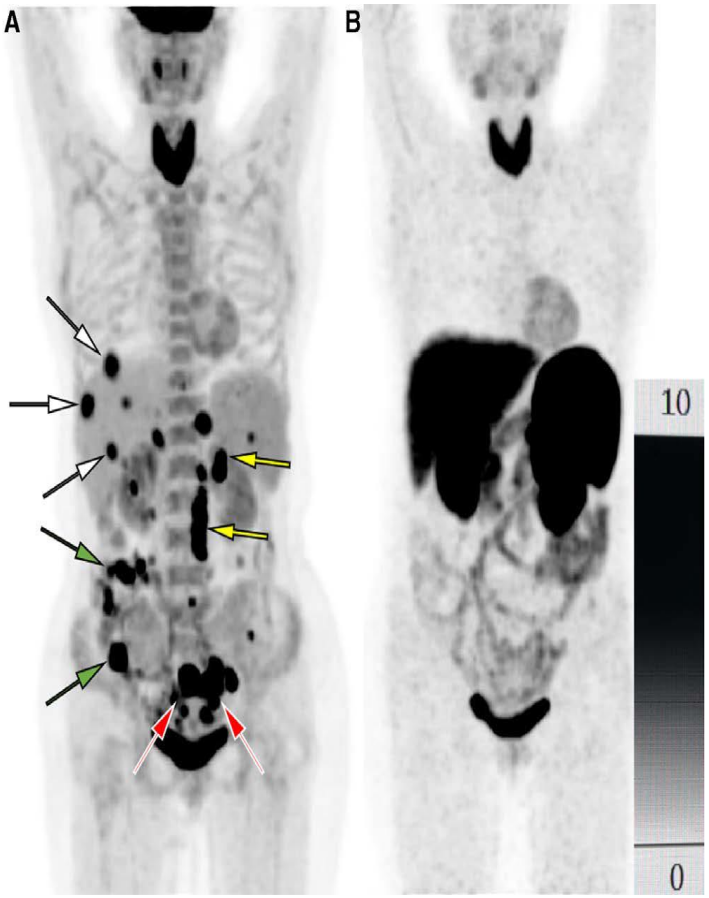

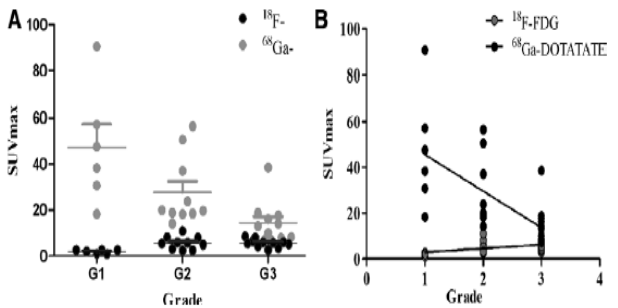

Figure 2. (A) The distribution of the maximum standard uptake value (SUVmax) of the lesions in patients with G1 to G3 grade neuroendocrine tumor, (B) The correlation between neuroendocrine tumor grade and SUVmax of ^{18}F-FDG and ^{68}Ga-DOTATATE PET/CT. ^{18}F-FDG = fluorine-18 labeled fluorodeoxyglucose, CT = computed tomography, PET = positron emission tomography.

In conclusion, the value of 68Ga-DOTATATE PET/CT in the diagnosis and staging of NET is higher than that of 18F-FDG PET/CT in NETs, while the value of 18F-FDG PET/CT in NET cannot be ignored, and the combined application of the 2 tracers has critical clinical significance for the management of patients with NET. The SUVmax of 18F-FDG and 68Ga-DOTATATE PET/CT was closely related to their pathological grading; the former was positively related to the grading of NET, while the latter had a negative correlation.

A 53-year-old female patient was found to have increased radioactivity uptake in the liver (white arrows), retroperitoneum (yellow arrows), iliac vessels (green arrows) and sigmoid colon (red arrows) on 18F-FDG PET/CT (A) 1 year after the operation of stomach fundus neuroendocrine tumor, but was negative on 68Ga DOTATE PET/CT (B), which was subsequently proved to be sigmoid adenocarcinoma with multiple metastases by pathology. CT = computed tomography, PET = positron emission tomography.

18F-FDG PET/CT & 68Ga-FAPI PET/CT

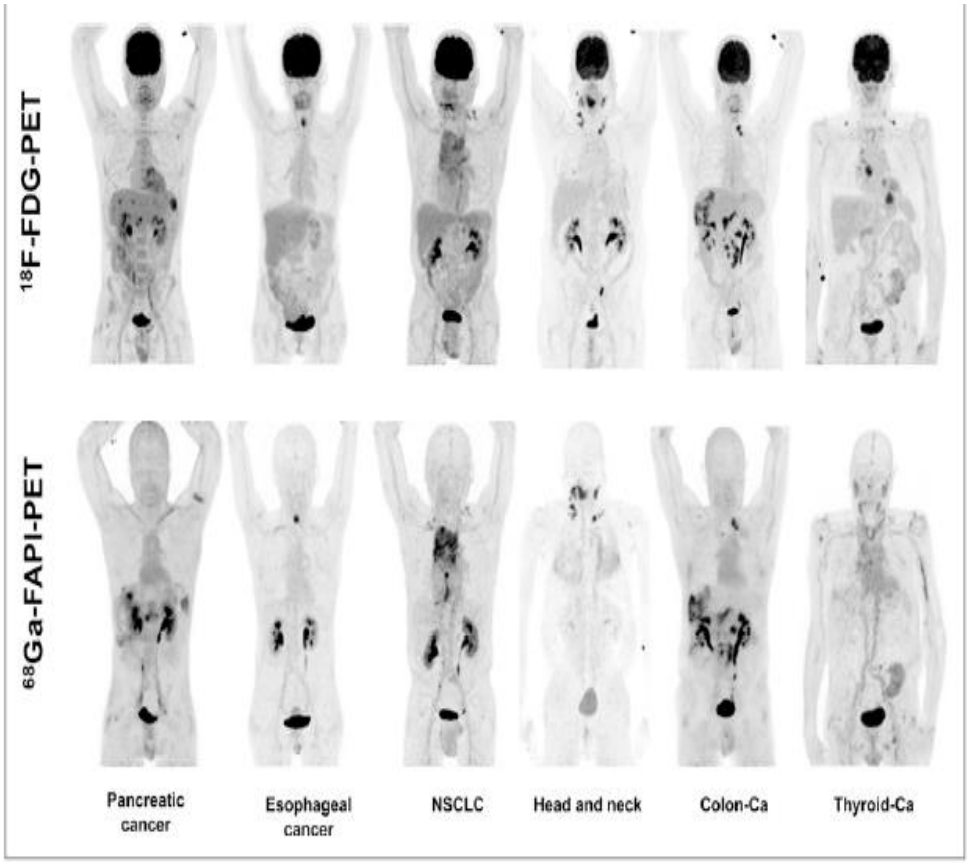

FIGURE 3. Intraindividual comparison of 6 patients with 6 different tumor entities undergoing ^{18}F-FDG PET and ^{68}Ga-FAPI PET imaging within less than 9 d. Five of 6 patients present similar strong tumor uptake with ^{18}F-FDG and ^{68}Ga-FAPI, and 3 of 6 could benefit from lower background in liver or pharyngeal mucosa. In contrast, iodine-negative thyroid cancer patient presented only minor ^{68}Ga-FAPI tracer uptake compared with ^{18}F-FDG. Ca = cancer; NSCLC = non–small cell lung cancer.

Fibroblast activation protein (FAP) is highly expressed in the stroma of several tumor entities. Especially breast, colon, and pancreatic carcinomas are characterized by a strong desmoplastic reaction, which means that 90% of the gross tumor mass can consist of stromal but not tumor cells.

68Ga-FAPI PET/CT is a promising new diagnostic method for imaging various kinds of cancer, in particular pancreatic, head and neck, colon, lung, and breast cancer, with tumor-to-background contrast ratios equal to or even better than those of 18F-FDG.
The favorable characteristics of the new ligands include fast tracer kinetics that seem appropriate for imaging patients even less than 1 h after injection; low background uptake in liver, oral mucosa, and brain; and independence from blood sugar. Because the 68Ga-FAPI tracers contain the universal DOTA-chelator, a theranostic approach—after labeling the ligand with an appropriate therapeutic radionuclide—also seems feasible.

2019-THE JOURNAL OF NUCLEAR MEDICINE-Frederik

Ga-PSMA

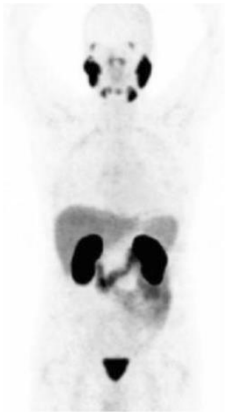

Physiological biodistribution of 68Ga-PSMA (PSMA 11). Salivary glands, small bowel (jejunum), kidneys, spleen, and liver are the organs with the highest uptake of 68Ga-PSMA-11

Names: [^{68}Ga] prostate-specific membrane antigen ligand; ^{68}Ga-PSMA

Biodistribution and metabolism (Fig. 25)

Prostate specific membrane antigen (PSMA), a tumour-associated antigen and type II transmembrane protein, is expressed on the membrane of prostatic epithelial cells and overexpressed on prostate tumour cells. Upon internalisation of the radiotracer, PSMA-expressing tumour cells can be detected during PET imaging (Heidenreich et al. 2014; Afshar-Oromieh et al. 2016; Demirci et al. 2016).

Scan acquisition

- Fasting of 4 h is suggested
- 2 or 3 MBq\Kg of ^{68}Ga-PSMA iv
- Uptake time 60–100 min
- Acquisition starts from the pelvis

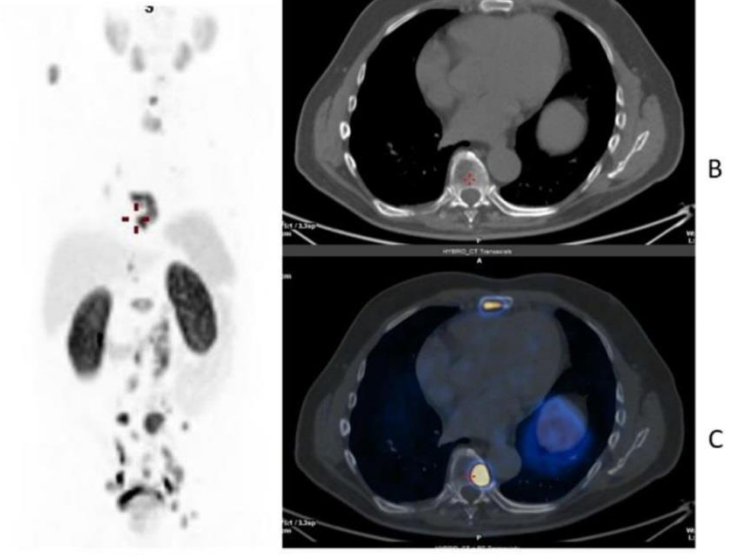

A B C

68Ga-PSMA, prostate cancer, staging. Clinical history: 56 y.o. man with prostate cancer. At presentation, Gleason score 4 + 5; PSA = 14 ng/ml, candidate to radical prostatectomy. PET/CT findings:
multiple foci of increased uptake involving prostate, lymph nodes, and bones (a MIP). Vertebral lesion seen on fused images (c) is not evident on CT (b) Fig.

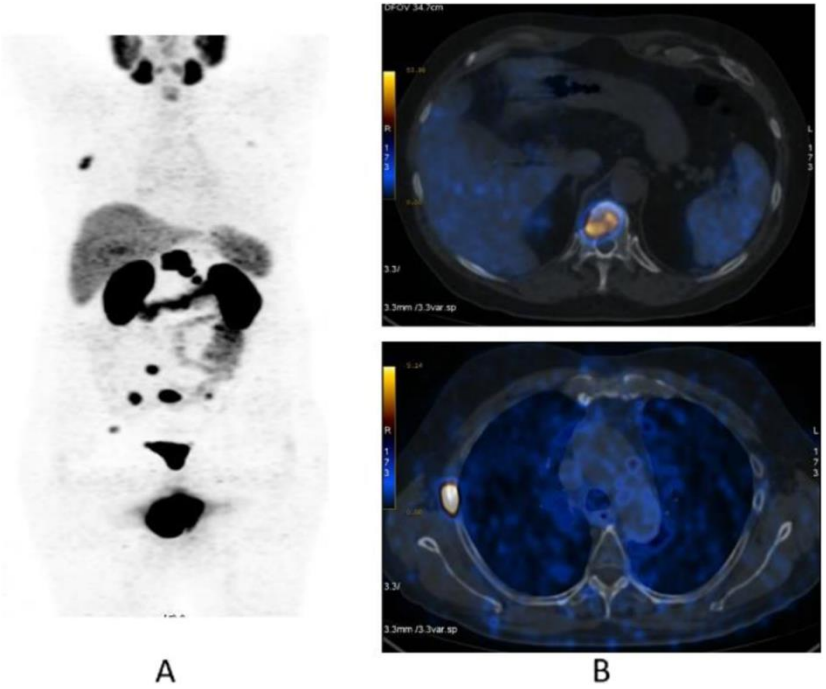

A B

68Ga-PSMA, prostate cancer, biochemical recurrence (BCR): 223Ra feasability. Clinical history: 72 y.o. man with prostate cancer, radical prostatectomy as primary treatment Gleason score 4 + 3; during abiraterone treatment, PSA increased up to 127 ng/ml, candidate to 223Ra chloride. PET/CT findings:
multiple foci of increased uptake in the bones. No lymph node or visceral metastases. After 68Ga-PSMA PET/CT, the patient has been referred to 223Ra chloride treatment. a MIP; b fused images

2019-European Journal of Hybrid Imaging-Giammarile

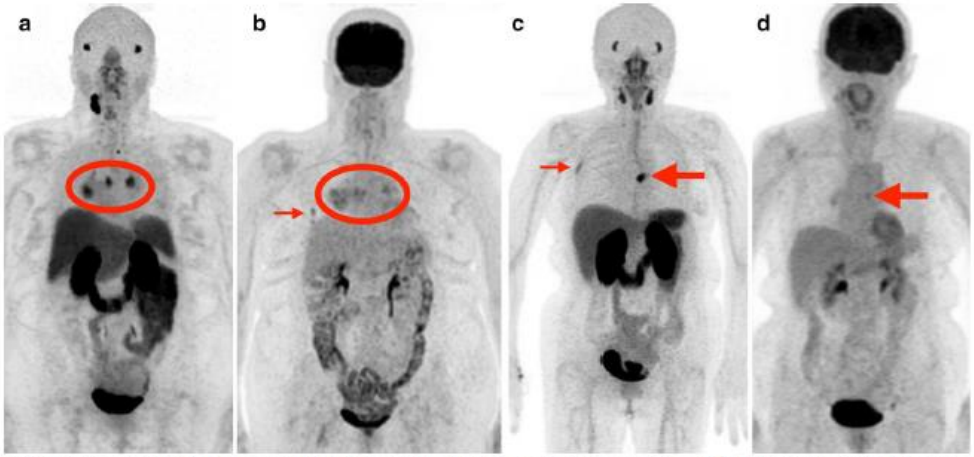

Fig. 3 Patients with metastatic thyroid cancer with greater PSMA uptake than FDG uptake: examples. **a**, **b** [^{68}Ga]Ga-PSMA-11 PET MIP (**a**) and 2-[^{18}F] FDG PET MIP (**b**) in a patient (Patient 6) with poorly differentiated papillary thyroid carcinoma. Bilateral hilar and mediastinal metastases (circled) are more avid on PSMA (median SUVmax 8.5) than FDG (median SUVmax 4.1). However, a small right middle lobe metastasis seen on FDG (B, small arrow) is not visible on PSMA. C–D: [^{68}Ga]Ga-PSMA-11 PET MIP (**c**) and 2-[^{18}F]FDG PET MIP (**d**) in a patient (Patient 5) with follicular thyroid carcinoma. A left 8th costovertebral junction metastasis (large arrows) is more avid on PSMA (SUVmax 15.0) than on FDG (SUVmax 3.5). In addition, a focus of uptake in the lateral right 4th rib (**c**, small arrow) is only visible on PSMA PET and may represent an additional site of metastatic disease

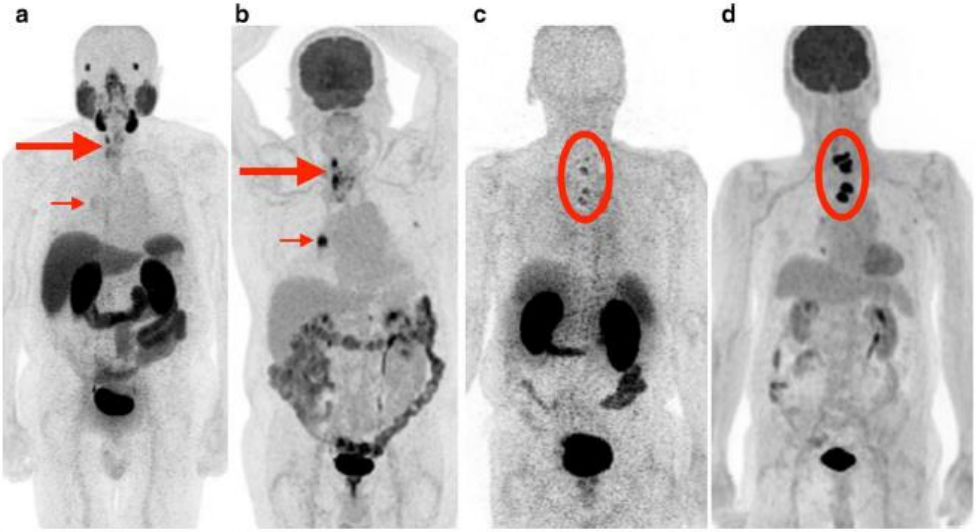

Fig. 4 Patients with metastatic thyroid cancer with greater FDG uptake than PSMA uptake: examples. **a**, **b** [^{68}Ga]Ga-PSMA-11 PET MIP (**a**) and 2-[^{18}F] FDG PET MIP (**b**) in a patient (Patient 4) with anaplastic thyroid carcinoma. Thyroid bed recurrence (large arrows) and right hilar nodal metastasis (small arrows) are more avid on FDG (median SUVmax 14.3) than PSMA (median SUVmax 3.3). **c**, **d** [^{68}Ga]Ga-PSMA-11 PET MIP (**c**) and 2-[^{18}F]FDG PET MIP (**d**) in a patient (Patient 1) with papillary thyroid carcinoma. Multiple lower cervical and upper thoracic vertebral body metastases (circled) are more avid on FDG (median SUVmax 21.1) than on PSMA (median SUVmax 9.0)

The main clinical application of ^{68}Ga-PSMA is in prostate cancer patients, namely initial diagnosis (Fendler et al. 2017), nodal staging (Schneider et al. 2016), restaging in case of biochemical recurrence (Calais et al. 2018; Maurer et al. 2016), and theranostic in case of ^{177}Lu-PSMA treatment (Mottet et al. 2011; Zamboglou et al. 2016), or alfa emitters such as ^{225}AcPSMA (Maurer et al. 2016).

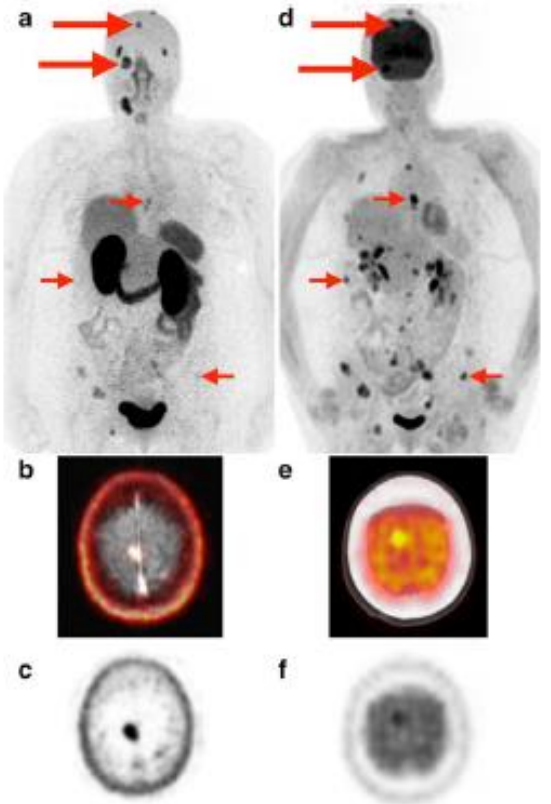

Fig. 5 Dural and skull base metastases.[^{68}Ga]Ga-PSMA-11 PET MIP (**a**) and 2-[^{18}F]FDG PET MIP (**d**) in a patient (Patient 2) with Hurthle cell carcinoma. Dural and skull base metastases (large arrows) are better delineated on PSMA PET due to lack of background brain uptake (example: right falcine dural metastasis better seen on fused axial PSMA PET/MRI (**b**) and axial PSMA PET (**c**) than on fused axial FDG PET/CT (**e**) and axial FDG PET (**f**). Extensive metastatic disease involving the left adrenal gland, ribs, thoracolumbar spine, and pelvis is better seen on FDG PET in this patient

C11

Carbon-11 is a PET radioisotope with a T1/2 of 20.334min. Due to the abundance of carbon in the chemistry of biomolecules, all C-11 radiopharmaceuticals demonstrate identical behaviour to natural compounds, allowing real tracing of the biological processes.

Production Method: C-11 can be produced in a cyclotron by bombarding nitrogen-14 with protons:

$^{14}N(p,\alpha)^{11}C$

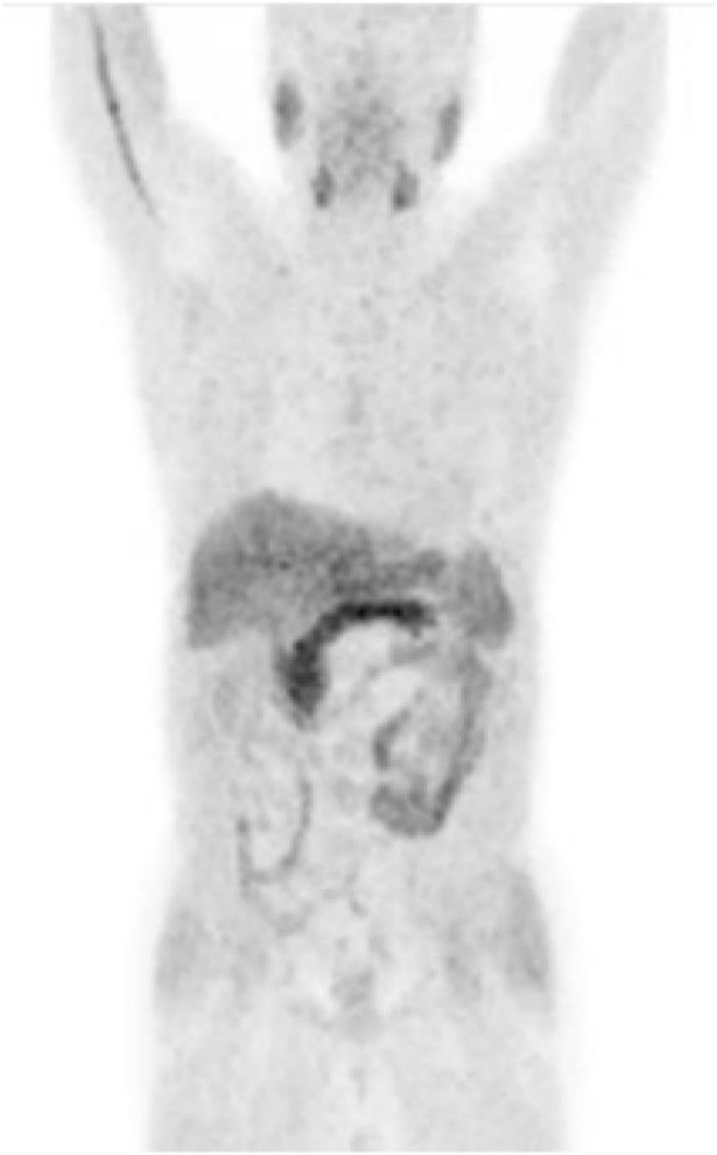

Physiological bio-distribution of 11C-acetate

Acetate
Names: CH3[11C]O2, 11C-acetate

- Fast of 4 h is suggested
- 4 or 5 MBq\Kg of ^{11}C-acetate iv
- Uptake time 10–20 min
- Acquisition starts from the pelvis

After injection ^{11}C-acetate is dispersed in many human tissues including the pancreas, bowels, liver, kidneys, and spleen. The tracer is not excreted in urine under normal circumstances. ^{11}C-acetate is typically incorporated into the cellular membrane in proportion to the cellular proliferation rate or alternatively oxidised to carbon dioxide and water. ^{11}C-acetate may also be converted into amino acids (Seltzer et al. 2004; Karanikas and Beheshti 2014).

2019-European Journal of Hybrid Imaging-Giammarile

The main clinical application of ^{11}C-acetate is the detection of non ^{18}F-FDG-avid neoplasm, such as differentiated hepatocellular carcinoma and renal cell carcinomas (Hain and Maisey 2003; Ho et al. 2003; Park et al. 2008). Some other applications of ^{11}C-acetate PET are brain tumours (Liu et al. 2006) and lung carcinomas, while in the past the tracer has been used in prostate cancer (Sandblom et al. 2006).

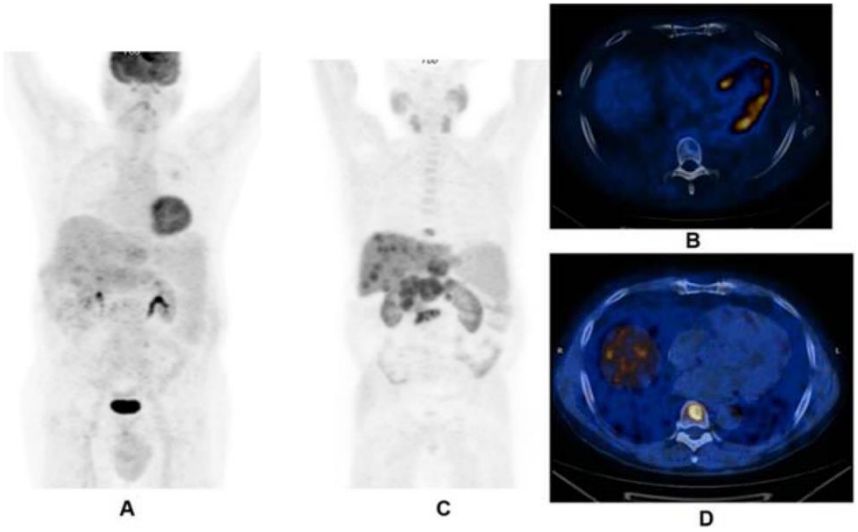

11C-acetate, staging hepatocellular carcinoma (HCC), comparison with 18F-FDG. Clinical history: 78 y.o. man with metastatic HCC after liver transplantation, patient underwent acetate and FDG study in a single day examination. PET/CT findings: acetate: multiple areas of increased uptake in the liver, lymph nodes, and bones consistent with lytic lesions at CT images. No FDG uptake. a FDG MIP. b FDG fused images. c acetate MIP. d acetate fused images

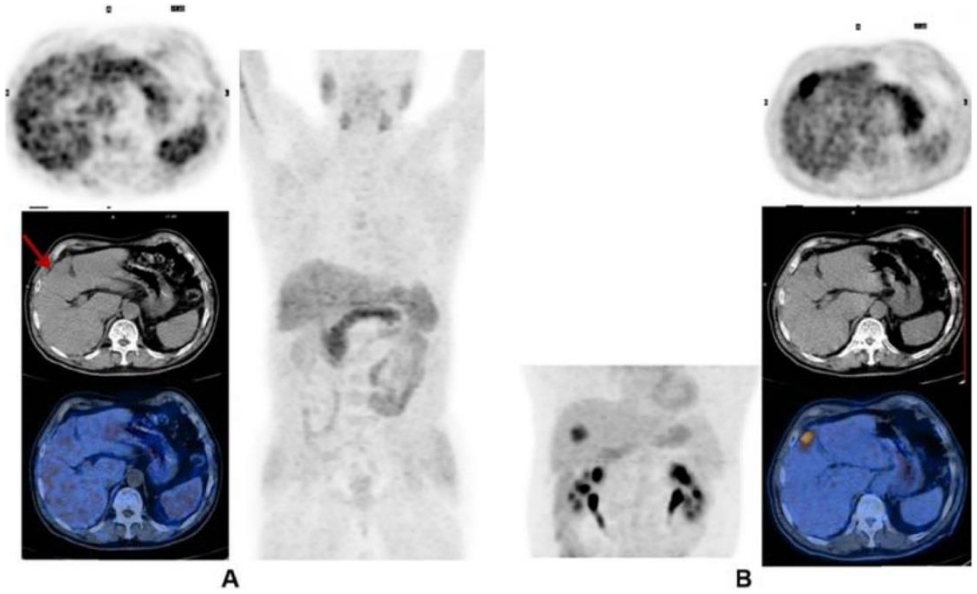

11C-acetate, staging hepatocellular carcinoma (HCC), comparison with 18F-FDG. Clinical history: 69 y.o. patients with HCC at presentation. Staging of a poorly differentiated HCC, patient underwent acetate and FDG study in a single day examination. PET/CT findings: acetate (a MIP and fused images): no areas of significant tracer uptake in the liver. The hypodense lesion in the IV segment (CT images red arrow) is consistent with the primary HCC. FDG (b MIP and fused images): increased tracer uptake in the IV segment (CT images red arrow) is consistent with the primary HCC

2019-European Journal of Hybrid Imaging-Giammarile

Methionine
Names: L-[methyl-11C] Methionine; 11C-Methionine

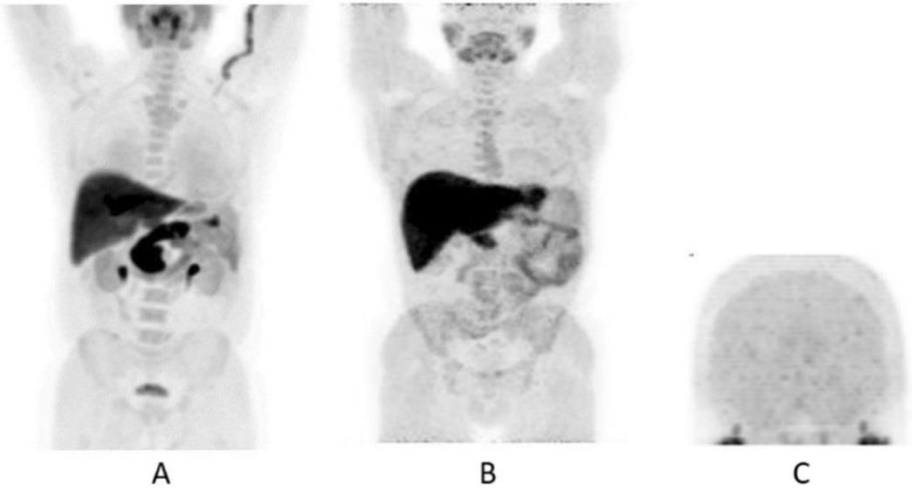

Physiological biodistribution of 11C-Methionine. MIP at 10 min (a) and 20 min (b) after administration; brain (c): there is only faint tracer uptake in the brain. There is low, variable uptake in the bowel. In most cases, no radioactive urine is detected in the ureters or bladder at 20 mins after injection

^{11}C-Methionine, an essential amino acid, enters the cells by various aminoacid transporters and is involved in the synthesis of proteins and lipids, as well as in the regulation and synthesis of DNA and RNA (Davis et al. 1982; Deloar et al. 1998; Harris et al. 2013).

- Fasting for at least 2 h
- 3 MBq/kg of ^{11}C-Methionine iv
- Injection immediately before the start of the emission

2019-European Journal of Hybrid Imaging-Giammarile

^{11}C-Methionine is used in the detection of brain tumours, primarily gliomas. The gliomas present an increased protein metabolism and capture ^{11}C-Methionine through specific carriers, in contrast to normal tissues that show low uptake.

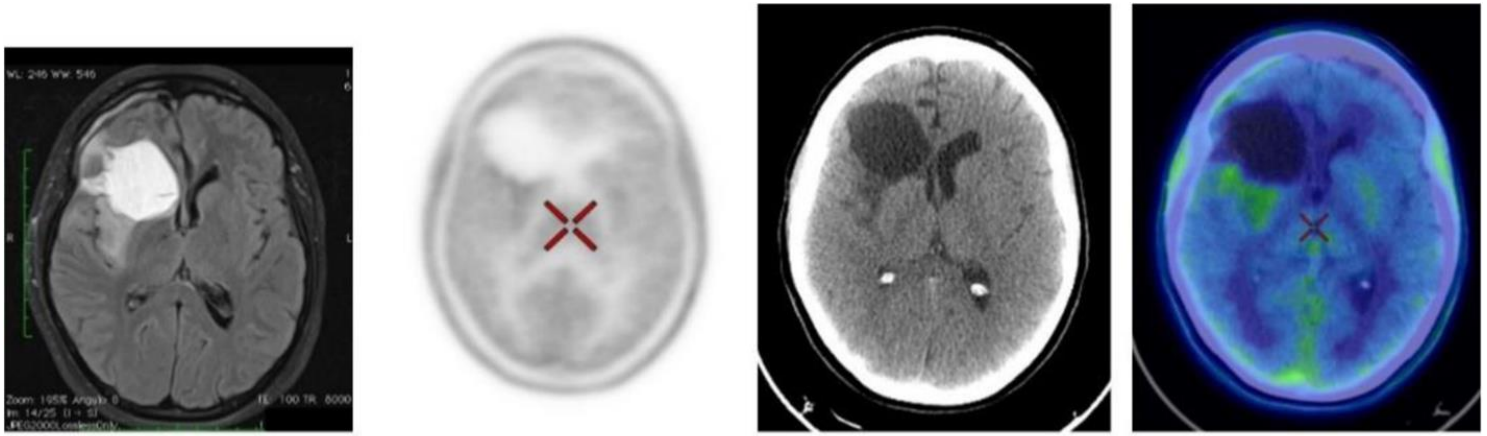

A B

11C-Methionine, Glioblastoma grade 2, surgical changes. Clinical history: 25 y.o. female. Glioblastoma grade 2. Surgical treatment with macroscopically complete resection of right frontal glioblastoma. MRI: T2-FLAIR image shows heterogeneous hyperintensity (a) and T1 using Gd shows peripheral contrast enhancement. PET/CT findings: slight tracer uptake in margins of surgical field, compatible with inflammatory activity in PET/CT images (b)

2019-European Journal of Hybrid Imaging-Giammarile

Choline
Names: 1. [11C]CH, 11C-choline
2. [18F]CH, 18F-fluorocholine

After injection, the tracer rapidly clears from the circulation (< 3 min), with high clearance by liver and kidneys. Increased metabolism will lead to an increased uptake of choline in the cell membranes and tissues.

^{11}C-choline distributes mainly to the pancreas, kidneys, liver, spleen, and colon. Based upon the relatively low urinary excretion of radioactivity, renal distribution is predominantly to the organ itself, rather than via formation of urine.

The urinary excretion of ^{18}F-fluorocholine has been reported to be about 5% of the administered activity in female patients and 2% in male patients within 60 min after injection (Mitterhauser et al. 2005; DeGrado et al. 2001; DeGrado et al. 2002).

- Fasting of 4 h is suggested
- 4 or 5 MBq\Kg of ^{11}C-choline iv/300 MBq ^{18}F-fluorocholine iv
- Uptake time 2–5 min for ^{11}C-choline/30 min for ^{18}F-fluorocholine
- Acquisition starts from the pelvis for ^{11}C-choline/head-thorax for ^{18}F-fluorocholine

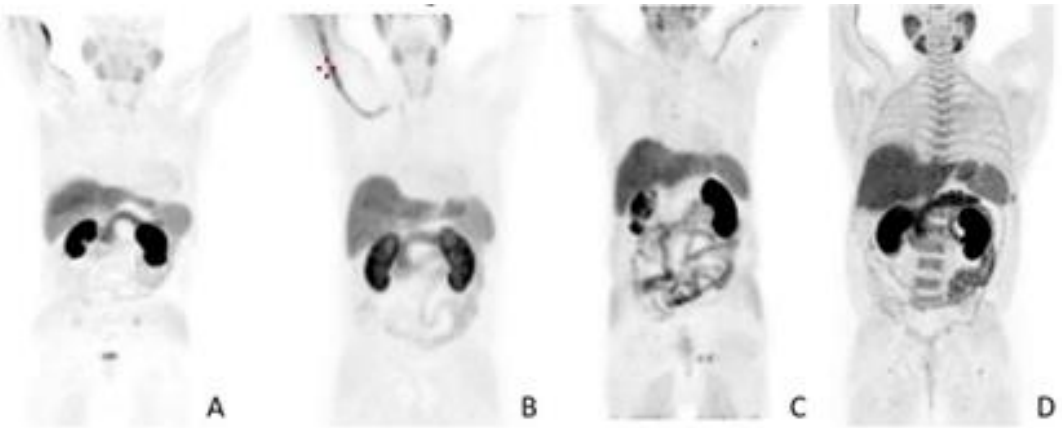

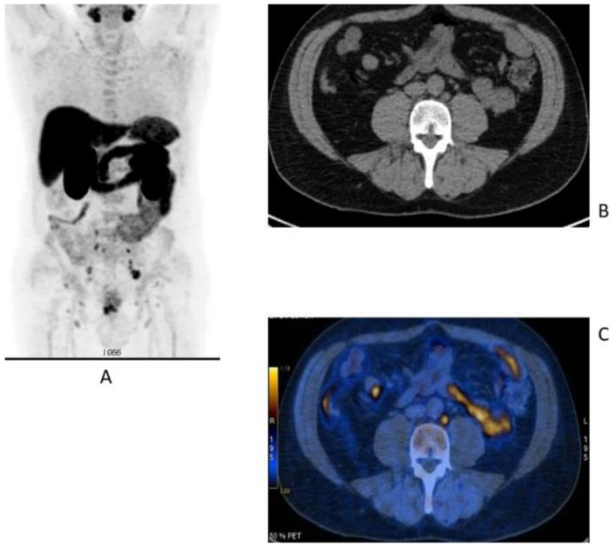

11C-choline, Initial staging: in very high-risk prostate cancer. Clinical history: 74 y.o. man with prostate cancer, Gleason score 4 + 5 according to biopsy. PSA = 126 ng/ml, T3a according to TRUS,candidate for radical prostatectomy. PET/CT findings: multiple foci of increased uptake seen through the pelvis and retroperitoneum, representing pathological uptake in the prostate and lymph node metastases.
However, there is no evidence of osseous or visceral involvement. MIP (a), CT (b), and fused images (c)

Physiological bio-distribution and normal variants of 11C-choline 2-5 min after administration: main findings. a Normal biodistribution but a small amount of radioactive urine is present in the bladder; mild uptake in the thyroid. b The presence of intense uptake in the vessels in which the tracers has been injected is a relatively common finding; some mild thyroid uptake is present. c Moderate uptake in the bowel may be present. d Some diffuse faint uptake in the bone marrow may be present especially after treatments as a bone marrow rebound

2019-European Journal of Hybrid Imaging-Giammarile

Choline

Names: 1. [11C]CH, 11C-choline
2. [18F]CH, 18F-fluorocholine

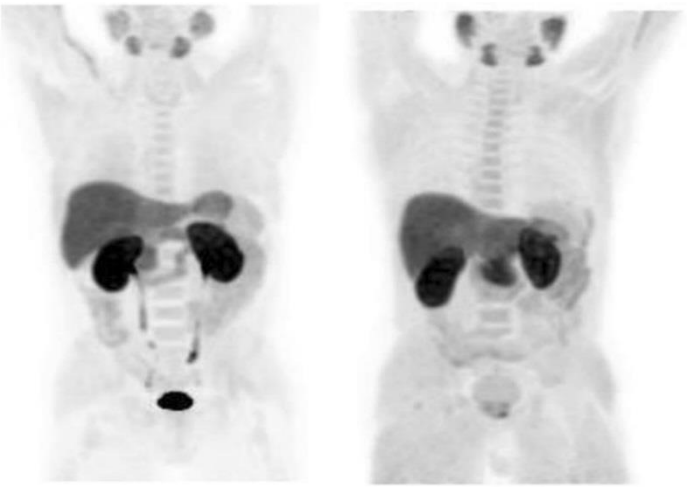

Physiological biodistribution of 18F-fluorocholine

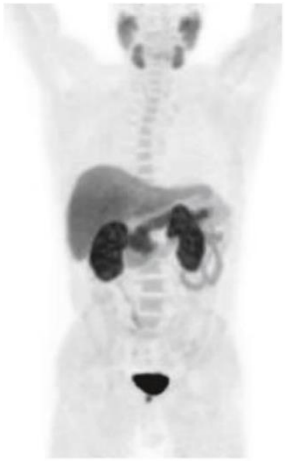

A

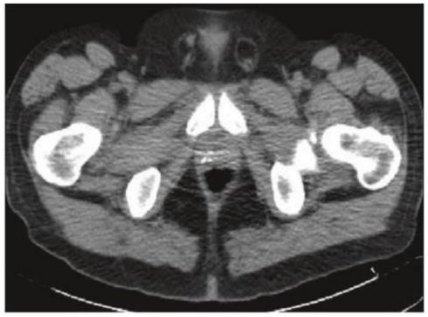

B

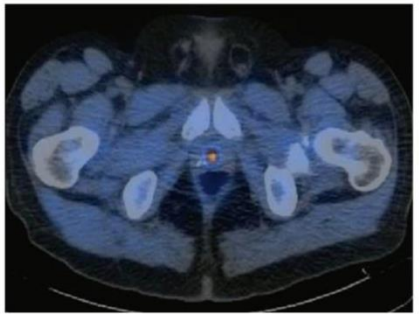

C

18F-fluorocholine, prostate cancer, biochemical recurrence (BCR). Clinical history: 72 y.o. man with prostate cancer, Gleason score 3 + 3, treated with radiation therapy. Patient underwent transuretral prostate resection prior to radiotherapy. BCR with a TTR 14 months and PSA 0.8 ng/ml PSAdt 13 months. PET/CT findings: focal increased uptake below the bladder seen on MIP (a), CT (b), and fused images (c)

2019-European Journal of Hybrid Imaging-Giammarile

C11-HTP

Names: [^{11}C] 5-hydroxytryptophan; ^{11}C-HTP

Biodistribution and metabolism (Fig. 44)

^{11}C-HTP is taken up into neuroendocrine tumours cells by L-large amino acid transporter followed by decarboxylation to serotonin. The resulting end-product is then transported into storage vesicles through the vesicular monoamine transporter as well as went through the metabolic pathway of serotonin (Addeo et al. 2018; Piccardo et al. 2012).

Scan acquisition

- No special diet is required
- 370 MBq of ^{11}C-HTP iv
- Uptake time 1 h

Clinical indications in oncology (Fig. 45)

^{11}C-HTP is used in the detection of neuroendocrine tumours. Since the uptake is related to the serotonergic pathway, ^{11}C-HTP is a possible alternative to ^{68}Ga-DOTA-peptide or ^{18}F-DOPA (Neels et al. 2006).

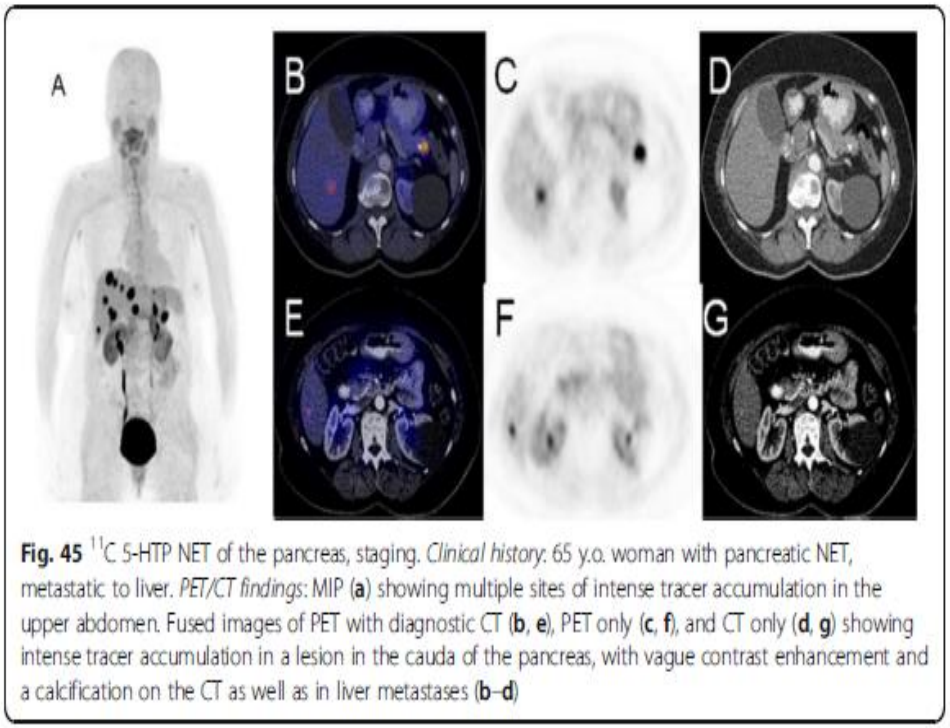

Fig. 45 ^{11}C 5-HTP NET of the pancreas, staging. *Clinical history*: 65 y.o. woman with pancreatic NET, metastatic to liver. *PET/CT findings*: MIP (**a**) showing multiple sites of intense tracer accumulation in the upper abdomen. Fused images of PET with diagnostic CT (**b**, **e**), PET only (**c**, **f**), and CT only (**d**, **g**) showing intense tracer accumulation in a lesion in the cauda of the pancreas, with vague contrast enhancement and a calcification on the CT as well as in liver metastases (**b**–**d**)

Somatostatin analogues

Names: [^{68}Ga] (1,4,7,10-tetraazacyclododecane-N, N′, N″, N‴-tetraacetic acid)-1- (d)-Phe1-Thy3-octreotate (DOTATATE)- (d)-Phe1-Thy3-octreotide (DOTATOC)- NaI3-octreotide (DOTANOC)

Biodistribution and metabolism (Fig. 46)

Synthetic somatostatin peptides show long biological half-life and stronger and more specific affinity for somatostatin receptors available on the cellular surface of neuroendocrine tumours. DOTATATE, DOTATOC, and DOTANOC have different affinities for receptor subtypes (Kroiss et al. 2013; Bergeret et al. 2019).

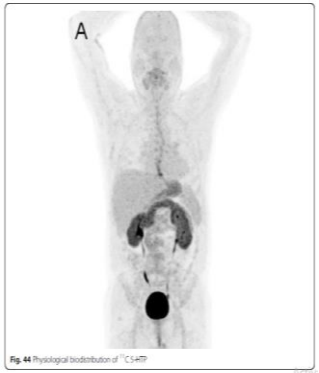

Scan acquisition

- No special diet is required
- 2–3 MBq\Kg of ^{68}Ga-DOTA-Peptide iv
- Uptake time 1 h

Clinical indications in oncology (Figs. 47, 48, 49, 50, 51, 52, 53, 54, 55, 56, 57, 58, 59, 60, 61, 62, 63, 64, and 65)

In the management of NETs ^{68}Ga-DOTA-conjugated peptide, PET/CT is used to localise primary tumours and detect sites of metastatic disease (staging); follow-up patients with known disease to detect residual, recurrent or progressive disease (re-staging); determine somatostatin status; monitor response to therapy; and select patients with metastatic disease for peptide receptor radionuclide therapy (Skoura et al. 2016; Sundin 2018; Singh et al. 2018; Waseem et al. 2019).

2019-European Journal of Hybrid Imaging-Giammarile

Amyloid PET in Imaging Neurodegenerative Disorders

Amyloid beta (Aβ, Abeta or beta-amyloid) denotes peptides of 36–43 amino acids that are the main component of the amyloid plaques found in the brains of people with Alzheimer's disease

Summary Guidelines for Interpretation of Amyloid PET Scans Using Different Tracers

Tracer category	Tracer name	Dose and acquisition protocol (clinical)	Visualization	Interpretation criteria for positive scan
Food and Drug Administration–approved	^{18}F-florbetaben	~300 MBq; 15- to 20-min acquisition beginning at 45–130 min (research use, 20-min acquisition beginning at 90–110 min)	Gray scale; window images to optimize GM/WM contrast in cerebellum	Increased GM uptake extending to cortical margin involving most slices in at least 1 of 4 target cortical regions: frontal, parietal, precuneus/posterior cingulate, lateral temporal; regional cortical tracer uptake/brain amyloid plaque load scores (*20*)
	^{18}F-florbetapir	~370 MBq; 10- to 20-min acquisition beginning at 30–50 min (package insert guidelines) for clinical use or 50–70 min (optimized kinetics for quantification) for research use	Inverse gray scale; window images to optimize GM/WM contrast in cerebellum	Loss of GM/WM contrast due to increased cortical binding in, first, 2 or more brain areas (each larger than single gyrus) with reduced or absent GM/WM contrast or, second, 1 or more areas with intense signal where GM > WM
	^{18}F-flutemetamol	~185 MBq; 10- to 20-min acquisition at 60–120 min (research use, 20-min acquisition at 90–110 min)	Color scale (NIH); normalize so that pons is at 90% of activity	Increased GM uptake (>50%–60% peak intensity) or loss of GM matter contrast in at least 1 of 4 cortical regions and 1 subcortical region: frontal, inferolateral parietal, precuneus/posterior cingulate, lateral temporal, striatum
Research	^{11}C-PiB	~555 MBq; dynamic 60- to 90-min acquisition (distribution volume ratio) or 20-min acquisition at 50–70 min (SUV ratio)	Color scale (NIH); window images to optimize GM/WM contrast in cerebellum	No formal guidelines for reading (research use only)
	^{18}F-flutafuranol	~185 MBq; 20- to 30-min acquisition beginning at 40–50 min	Color scale (NIH); window images to optimize GM/WM contrast in cerebellum	No formal guidelines for reading (research use only)

GM = gray matter; NIH = National Institutes of Health; WM = white matter.

2022-jnm-Chapleau

Amyloid PET in Imaging Neurodegenerative Disorders

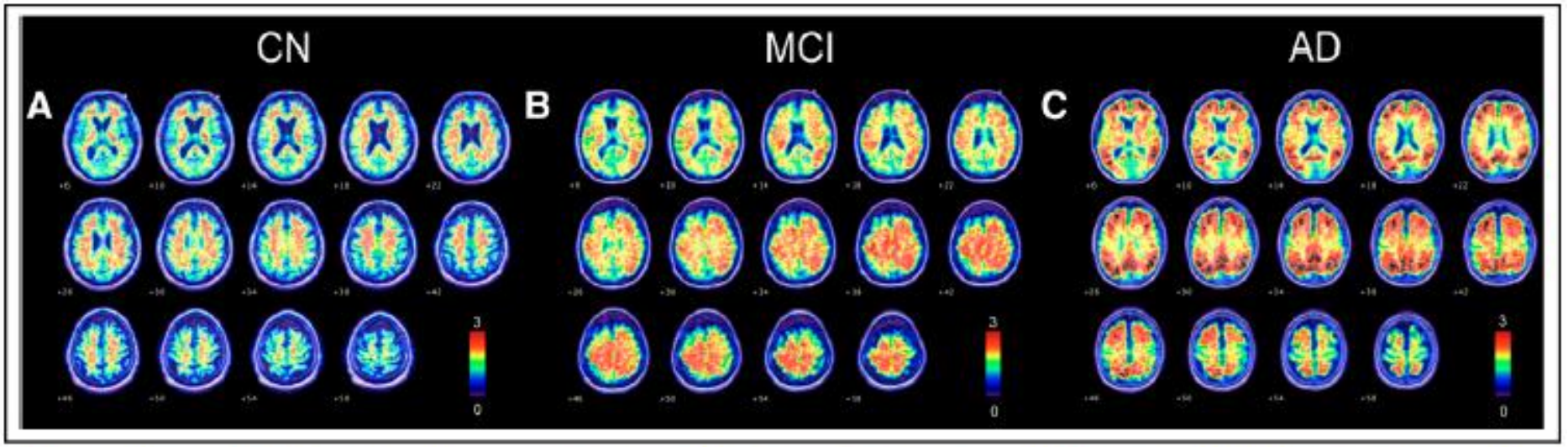

FIGURE 4. Evolution of amyloid PET positivity across AD spectrum. (A) Positive ^{11}C-PiB scan of cognitively normal (CN) participant, in which significant binding is observed in precuneus, posterior cingulate cortex, and medial prefrontal areas. (B) Positive ^{11}C-PiB scan of MCI patient, in which significant and moderate binding is observed throughout cortex. (C) Positive ^{11}C-PiB scan of AD patient, in which significant and severe binding is observed throughout cortex.

mild cognitive impairment (MCI)
Pittsburgh compound B(PiB)

COPPER-64: GENERAL AND PHYSICAL PROPERTIES FOR PET IMAGING

Copper (Cu) is a transition metal with atomic number 29, and an important trace element for most organisms. In humans, copper plays a role as a cofactor for numerous enzymes, such as Cu/Zn-superoxide dismutase, cytochrome-c oxidase, tyrosinase, ceruloplasmin, and other proteins, crucial for respiration, iron transport and metabolism, cell growth, and hemostasis.[65,66] For widespread use in medicine of any radioisotope, 2 factors are essential: availability of the isotope and a stable and effective mode of binding with an appropriate chemical carrier.[67] Selection of the proper radionuclide in radiopharmaceutical design is critical and depends on several factors, including the half-life of the radionuclide, which should allow sufficient uptake and distribution to yield considerable contrast and quality images. The energies of the radionuclide emission should be appropriate for proper detection by the equipment, whereas cost and availability are also important considerations.[68] Natural copper comprises 2 stable isotopes, ^{63}Cu (69.17%) and ^{65}Cu (30.83%), and 27 known radioisotopes; 5 of them are particularly interesting for molecular imaging applications (^{60}Cu, ^{61}Cu, ^{62}Cu, and ^{64}Cu), and in vivo targeted radionuclide therapy (^{64}Cu and ^{67}Cu).[67]

^{64}Cu-labeled molecules are promising imaging agents for PET due to the favorable nuclear characteristics of the isotope (half-life = 12.7 hours, β+ 17.8%, maximum energy (Emax) = 0.655 MeV, β− 38.4%, Emax = 0.573 MeV) and its availability in high specific activity.[68] The longer physical half-life of ^{64}Cu compared to ^{68}Ga (68.73 h) (**Table 1**), ^{11}C (20 minutes) and ^{18}F (110 minutes) enables imaging at delayed time points, which allows sufficient time for clearance from background tissues, resulting in increased image contrast, particularly for targeting agents that demonstrate long circulation times, such as antibodies and nanoparticles.[69]

Cu64

Production Method: Cu-64 is typically produced in a cyclotron through the irradiation of zinc-64 with protons:

$^{64}Zn(p,n)^{64}Cu$

Table 1
Decay characteristics of copper-64 and copper-67 in comparison to gallium-68

Isotope	Half-Life	β⁻ keV (%)	β⁺ keV (%)	EC (%)	ϒ keV (%)
^{64}Cu	12.7 h	573 (38.4)	655 (17.8)	43.8	511 (35.6)
^{68}Ga	67.83 min	1899 (87.8) 822 (1.2)	88.88 (41) —	41 —	511 (178) 1077 (3.2)
^{67}Cu	61.83 h	395 (45) 484 (35) 577 (20)	—	—	184 (40) — —

The longer half-life of 64Cu, compared with that of 68Ga, provides the significant advantage of late imaging up to 24 hours after administration of the radiopharmaceutical.
In addition, the longer half-life of 64Cu is compatible with the time scales required for the ability to create complex radiopharmaceuticals, and for the optimal biodistribution of slower-clearing agents, such as monoclonal antibodies, nanoparticles, and higher-molecular-weight polypeptides requiring longer imaging times, thereby allowing several applications in oncological and nononcological fields. Future diagnostic applications of 64Cu could possibly be enhanced with the use of the betaemitting 67Cu, which has been used in the treatment of other malignancies,85 as a therapeutic matched pair for radioligand therapy of prostate cancer.

[64Cu]DOTA-trastuzumab

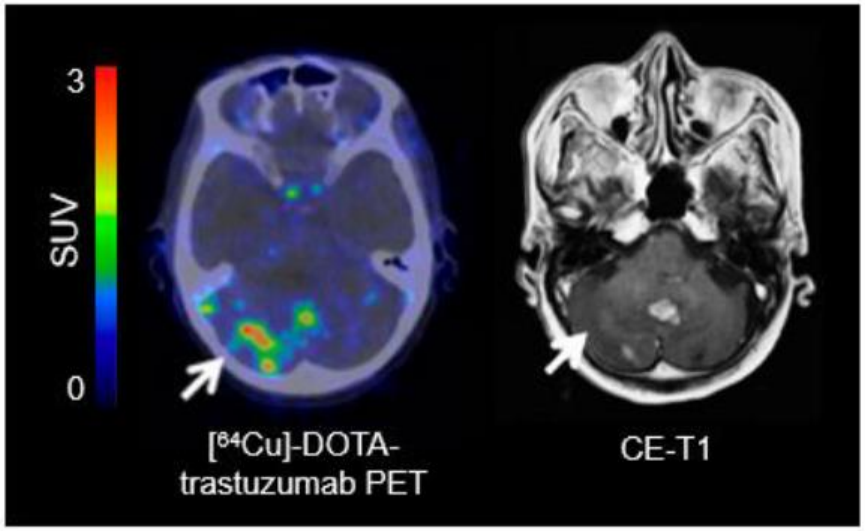

Figure 3. [^{64}Cu]-DOTA-trastuzumab positron-emission tomography (PET) and contrast-enhanced magnetic resonance imaging (MRI) performed one day after initiation of treatment with trastuzumab in a patient with a human epidermal growth factor receptor 2 (HER2)-positive breast cancer with brain metastases. In single brain metastases, [^{64}Cu]-DOTA-trastuzumab PET helps to improve lesion detection (arrow) (modified from Tamura et al. [160], with permission from the Society of Nuclear Medicine and Molecular Imaging).

Both the epidermal growth factor receptor (EGFR) and the human epidermal growth factor receptor 2 (HER2) are transmembrane protein receptors and belong to the EGFR family. These receptors are targets for various growth factors that mediate various cellular processes such as dierentiation or proliferation.

In clinical oncology, various gene mutations may lead to overexpression of these proteins and are associated with the development of a variety of cancers.For identifying EGFR overexpression, PET ligands such as [11C]erlotinib, [11C]PD153035, and [89Zr]Zr-DFO-nimotuzumab have been used . The most relevant PET tracers for imaging of HER2 overexpression are [64Cu]DOTA-trastuzumab and [89Zr]pertuzumab (Figure 3).

2020-molecules-Werner etal

correlation between [64Cu][Cu(ATSM) PET/CT results and expression of the hypoxia-inducible factor 1α (HIF-1α) expression, a marker of tissue hypoxia in a patient with Glioblastoma

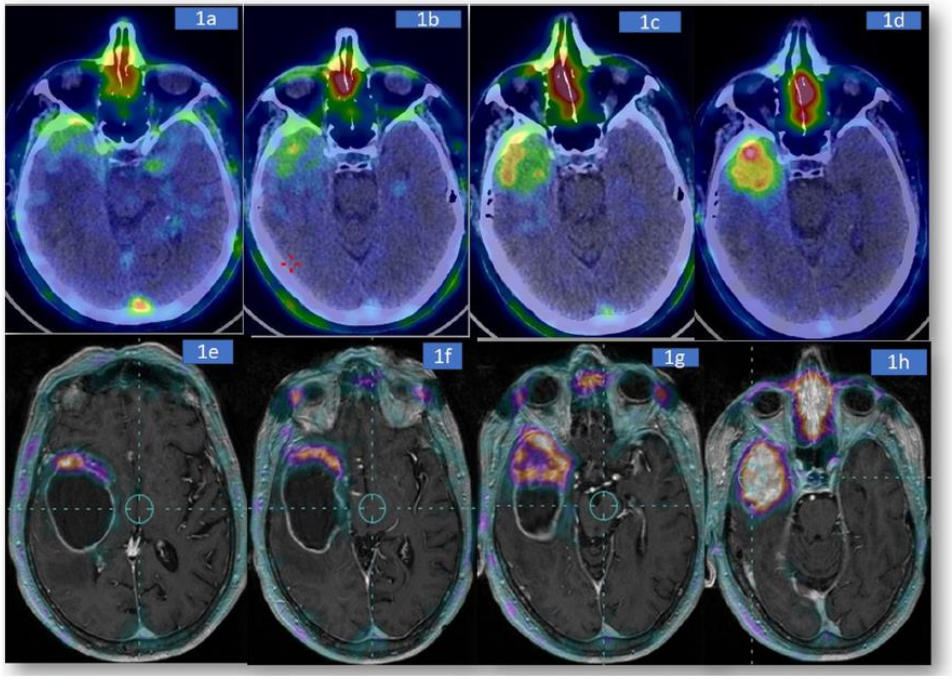

Fig. 1 PET/CT acquisition at different times after injection. Brain images taken at 5 min (**a**) 1, (**b**), 4 (**c**) and 18 h (**d**) post-radiotracer injection. Progressive and significant uptake of [^{64}Cu][Cu(ATSM)] into the lesion is documented during time. The SUVmax increases from 2.0 (5 min post-injection) to 4.9 (18 h post-injection). The heterogeneity of tumour is particular evident on PET-MRI fusion images obtained at 18 h. Images **e**-**h** represent different transaxial planes in cranio-caudal direction (upper (**e**) to lower (**h**) planes)

Glioblastoma multiform (GBM), a malignant brain tumour, has a very often poor prognosis. The therapeutic approach is represented by surgery followed by radiotherapy and chemotherapy. Hypoxia is a factor that causes a reduction of both radiotherapy and chemotherapy effectiveness in GBM and other cancers. Through the use of [64Cu][Cu(ATSM)], a hypoxia-targeting positron emission tomography (PET) radiotracer, is possible to identify the presence of hypoxic areas within a lesion and therefore modulate the therapeutic approach according to the findings.

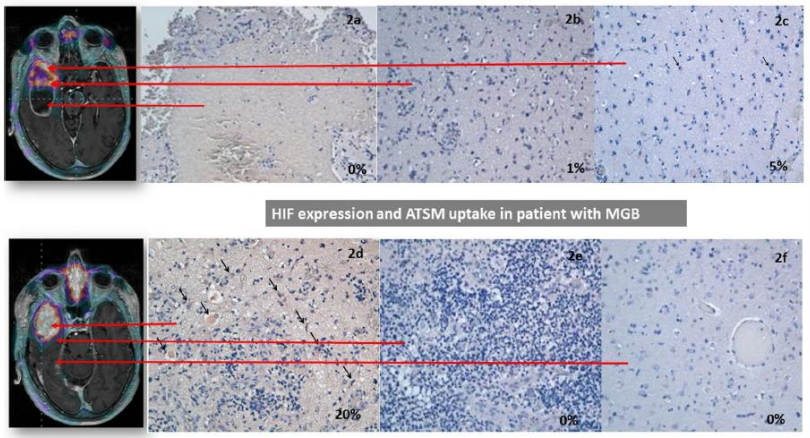

Fig. 2 Spatial correlation between [^{64}Cu][Cu(ATSM)] PET images and HIF-1α expression. **a** Necrotic area surrounded by neoplastic cells, no HIF-1α signal was detected. **b** High cellular neoplastic area, 1% of positive cells to HIF-1α. **c** Peripheral tumour area with lower cellularity, 5% of positive cells to HIF-1α corresponding to SUVmax of 2.7. **d** Central neoplastic area with HIF-1α expression in 20% of the cells (arrows) corresponding to SUVmax of 4.9. **e** Neoplastic area associated inflammatory infiltrate, no HIF-1α positive cells observed. **f**. Peripheral area adjacent to the tumour, reactive gliosis. Absent expression of HIF-1α. **a**-**f** The selection of the regions is based on manual reporting from the neurosurgeons

2019-BMC Cancer-Gangemi

64Cu-PSMA PET/CT

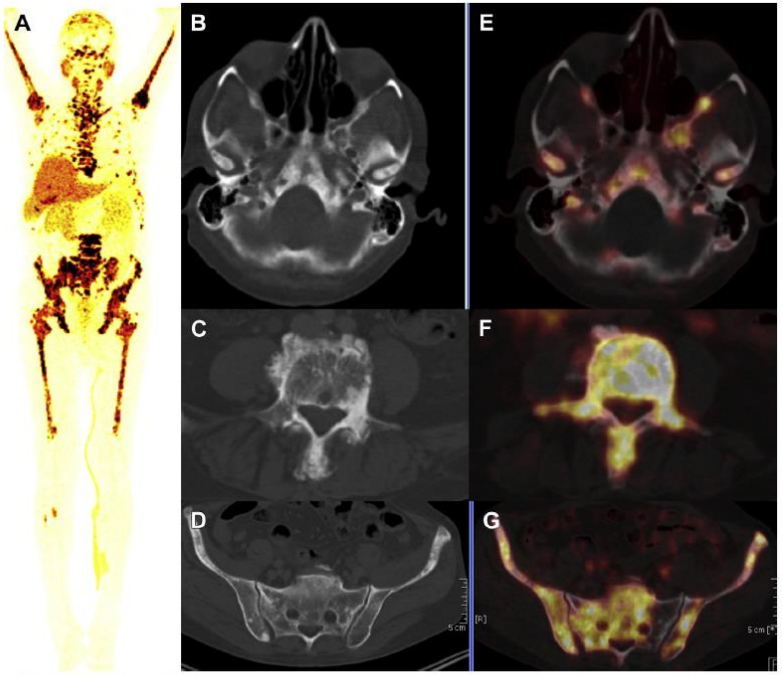

Fig. 1. ^{64}Cu-PSMA PET/CT demonstrates extensive axial and appendicular skeletal metastases. (*A*) MIP image. (*B–D*) Serial axial CT. (*E–G*) Corresponding PET/CT fusion images.

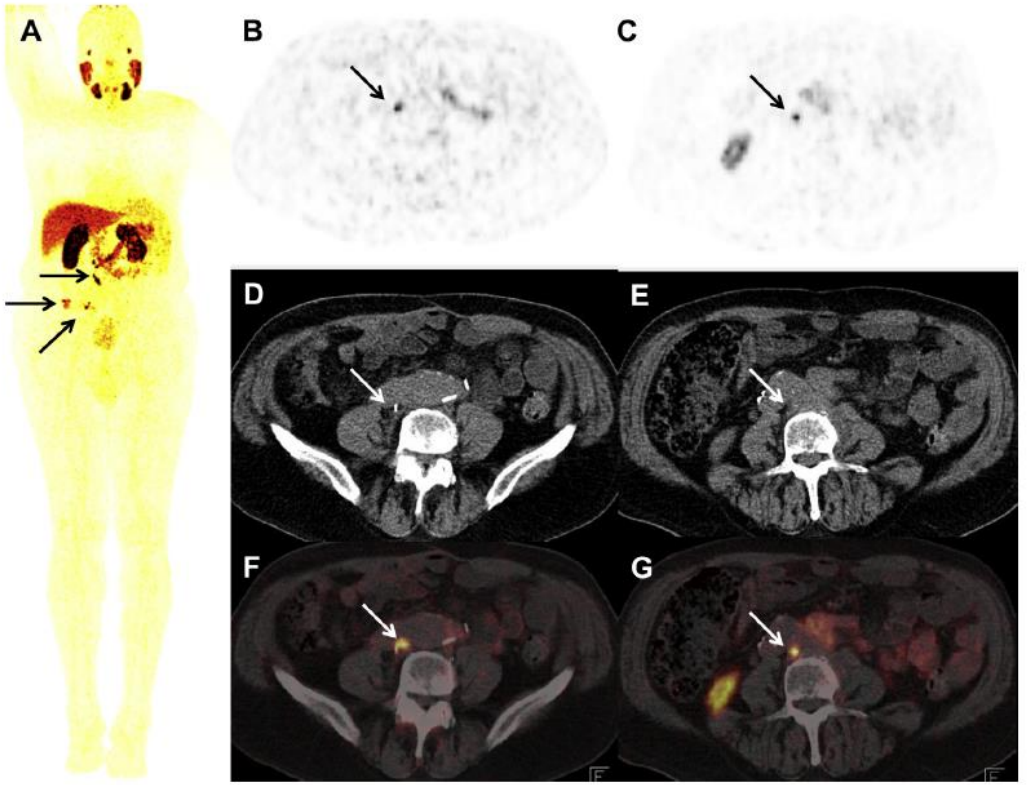

Fig. 2. Patient restaged with progressive disease. ^{64}Cu-PSMA PET/CT demonstrates multiple abdominopelvic lymph node metastases. (*A*) MIP image. (*B*, *C*) Axial PET images. (*D*, *E*) Corresponding CT. (*F*, *G*) PET/CT fusion images. Arrows indicate positive findings.

2017-PET Clin-singh

N13

Production Method: N-13 is produced by irradiating carbon-12 with protons in a cyclotron:

$^{12}C(p,n)^{13}N$
Half life:9.965min

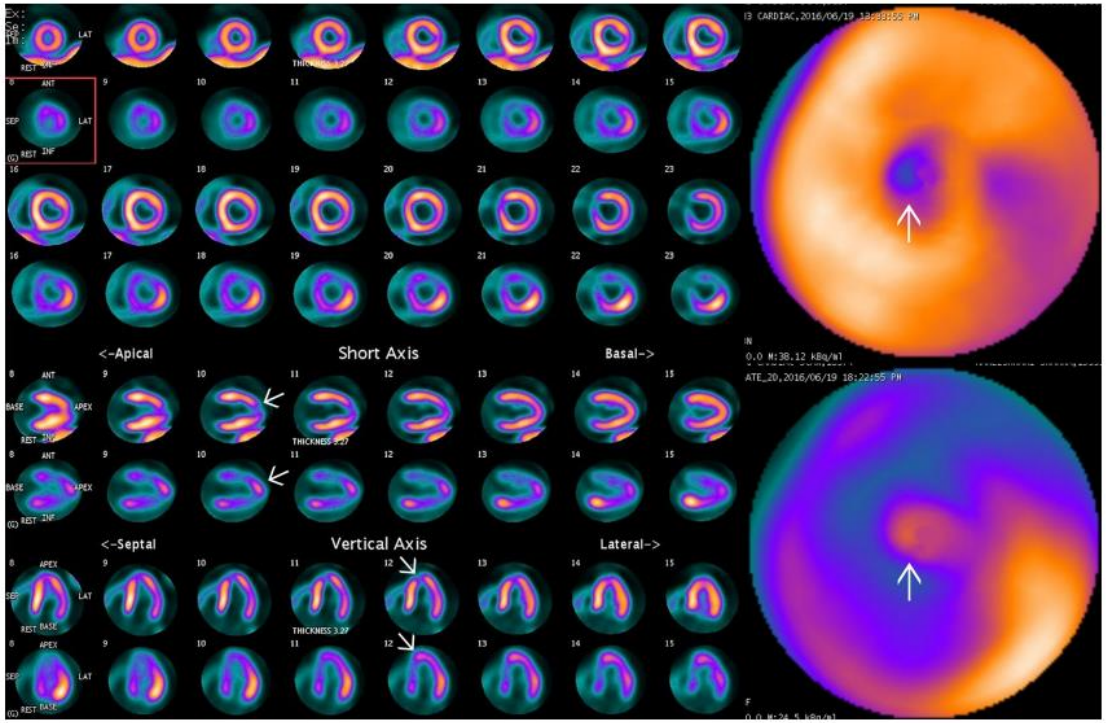

Figure 1. Rest PET-CT 13N ammonia perfusion (*top rows*) and 18F FDG metabolic images (*bottom rows*) displayed in standard short, vertical long, and horizontal long axis views. Perfusion images showing negligible tracer uptake in the apical region (*white arrow*) which on 2D polar map localized to the apex of heart, while metabolic images showing preserved FDG uptake in apical region (*white arrow*) suggestive of viable myocardium.

N13-ammonia(cardiac perfusion)
F-FDG(cardiac-viability)

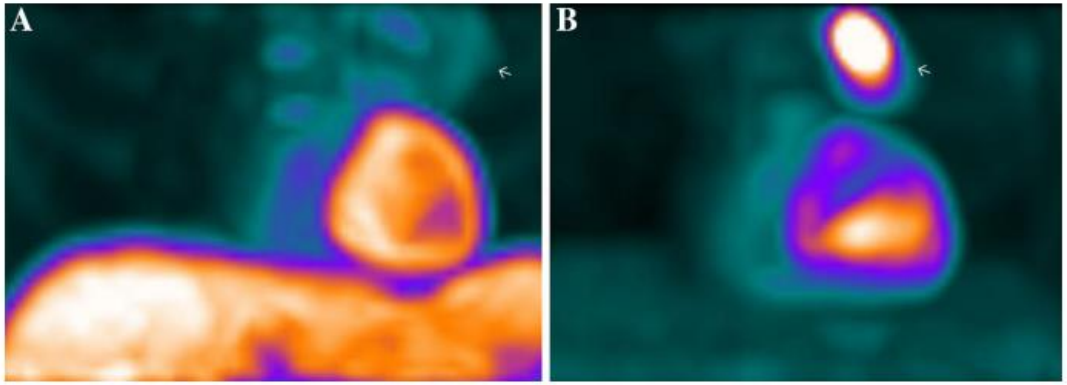

Figure 2. Rest planar projection images of N-13 ammonia showing physiological tracer uptake in the myocardium and liver, while faint tracer activity is noted in the mediastinal mass (**A**, *white arrow*) and the planar projection image of F-18 FDG showing intense FDG uptake in the mediastinal mass (**B**, *white arrow*) in addition to myocardial uptake.

2016-Journal of Nuclear Cardiology-malik

Rb-82

Production Method: Rb-82 is typically generated from a generator system where strontium-82 decays to rubidium-82:

$^{82}Sr \rightarrow {}^{82}Rb + \beta^-$

Half life:75sec

1. **Parent Isotope**: The Rb-82 generator system typically uses Strontium-82 (Sr-82) as the parent isotope. Sr-82 has a longer half-life of approximately 25.8 days and decays into Rb-82.

2. **Decay Process**: As Sr-82 decays, it produces Rb-82. The generator is designed to allow for the extraction of Rb-82 while maintaining a supply of Sr-82.

Many facilities find that a generator can be effective for about 2 to 3 months before replacement is necessary.

Rubidium-82 chloride (cardiac perfusion)

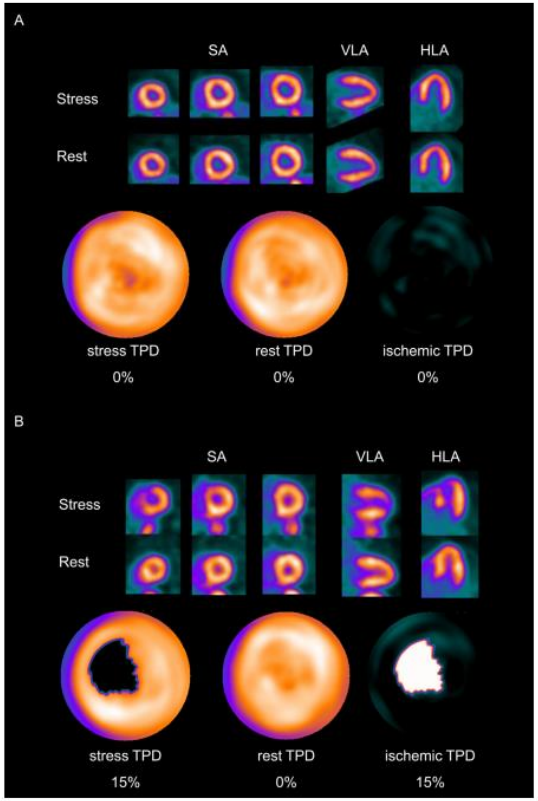

Figure 4.
PET images and quantitative polar maps from a patient with normal limits database (A). Uniform tracer distribution is noted with no quantitative abnormality. Abnormal PET images in patient with a 90% proximal LAD stenosis (B). A reversible perfusion defect is seen in the anterior, septal and apical walls both on the images and the polar maps. Stress and ischemic TPD were both 15%.

2012-J Nucl Cardiol. -Nakazato

a. ^{82}Rb PET/CT static perfusion analysis

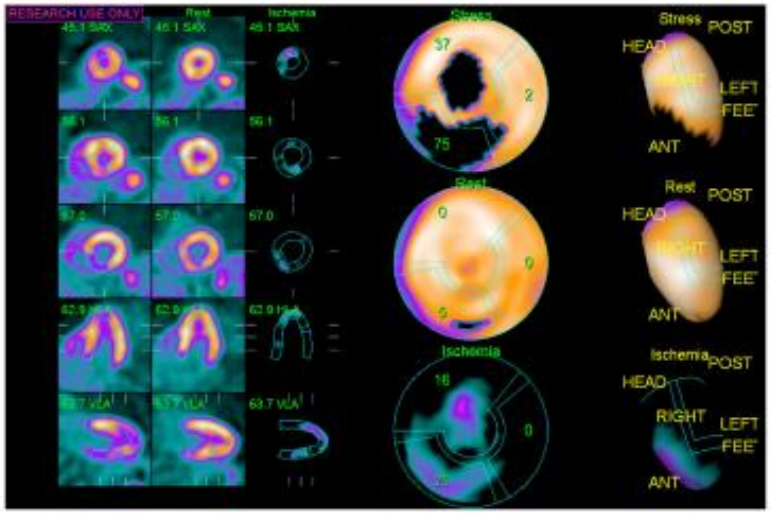

b. ^{82}Rb flow detection of 3VD

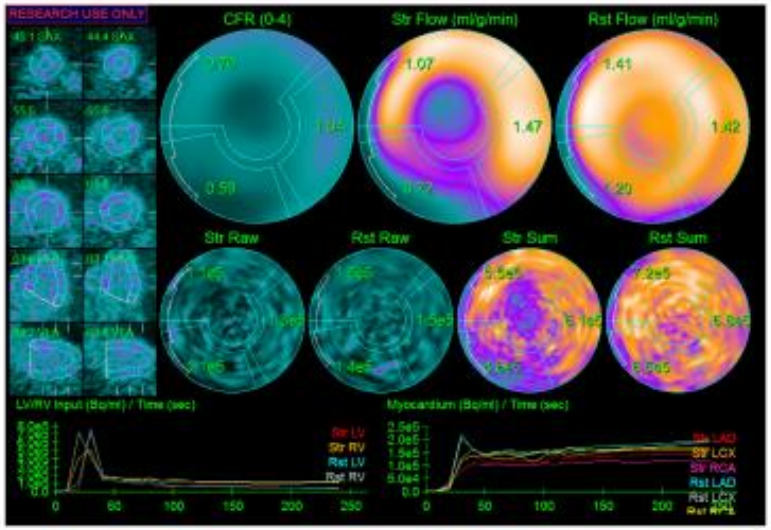

Fig. 7.
Example of added value of myocardial flow reserve over ischemia quantification for diagnosis from ^{82}Rb PET. Relative quantification of total perfusion deficit at stress and rest shows stress and ischemic abnormalities in left anterior descending (LAD) and left circumflex (LCX) territories but normal right coronary artery (RCA) territory (a), while

2014-Clin Transl Imaging-Slomka

O-15

Production Method: O-15 is also produced in a cyclotron by irradiating nitrogen-14 with protons:

$^{14}N(p,\alpha)^{15}O$

Half life:122.24sec

O15-O2(brain–cardiac)

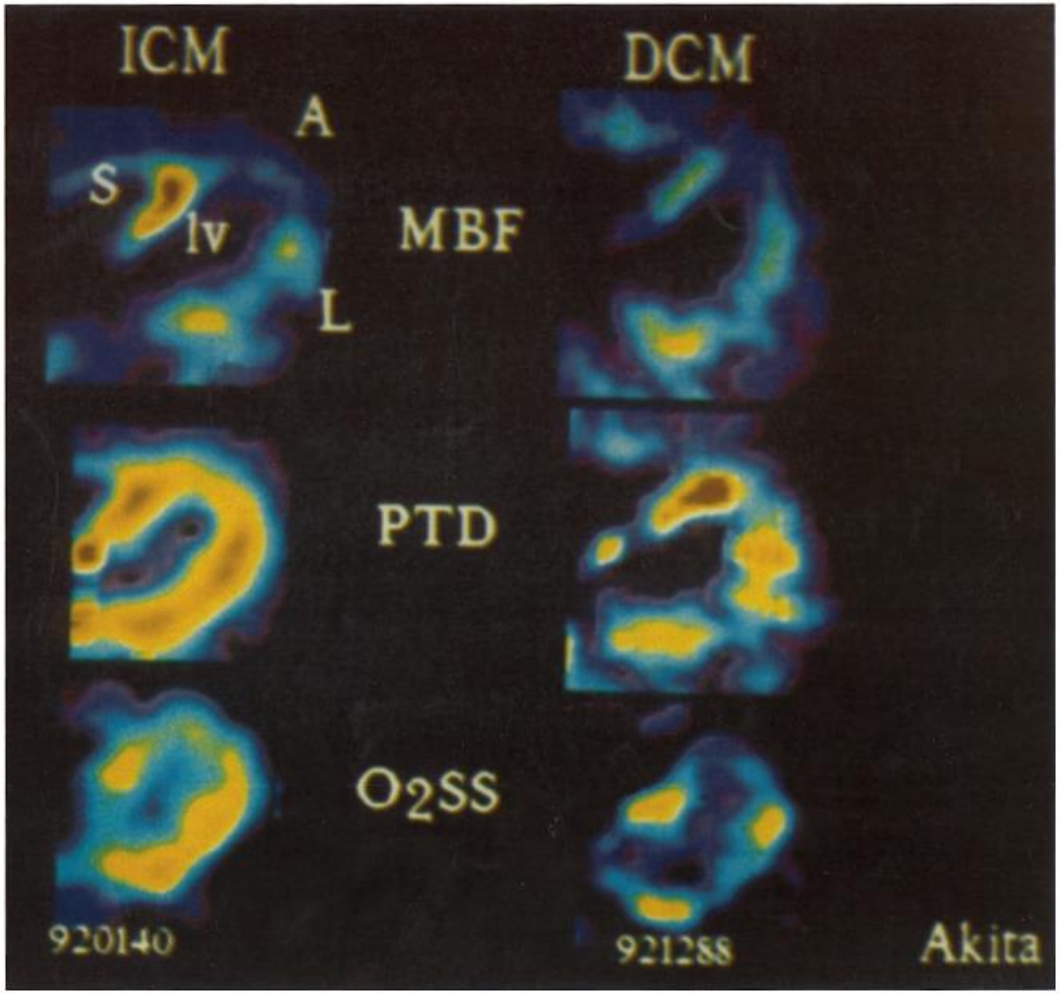

Fig. 1. A left midventricular transaxial slice of myocardial blood flow (MBF), perfusable tissue density (PTD), and oxygen steady state (O_2SS) PET images. For the patient with ICM, the figure shows a dilatation of the left ventricle and a large defect in MBF distribution in the anterior and lateral wall regions. The reduction in MBF is less important in the lateral wall than in the anterior wall region. The oxygen steady state distribution is more impaired in the anterior than in the lateral walls. For the patient with DCM, the figure shows a large dilatation of the LV, heterogenous distributions of MBF and O_2SS. The PTD images are provided to select regions of interest on the left ventricle in each patient (PTD images can be derived from a set of 15-0_2 water dynamic scans obtained simultaneously with the MBF quantitation). S, septum; A, anterior; L, lateral; lv, left ventricle.

2001-CLINICAL NUCLEAR MEDICINE-agostini

O15-water(cerebral blood flow)

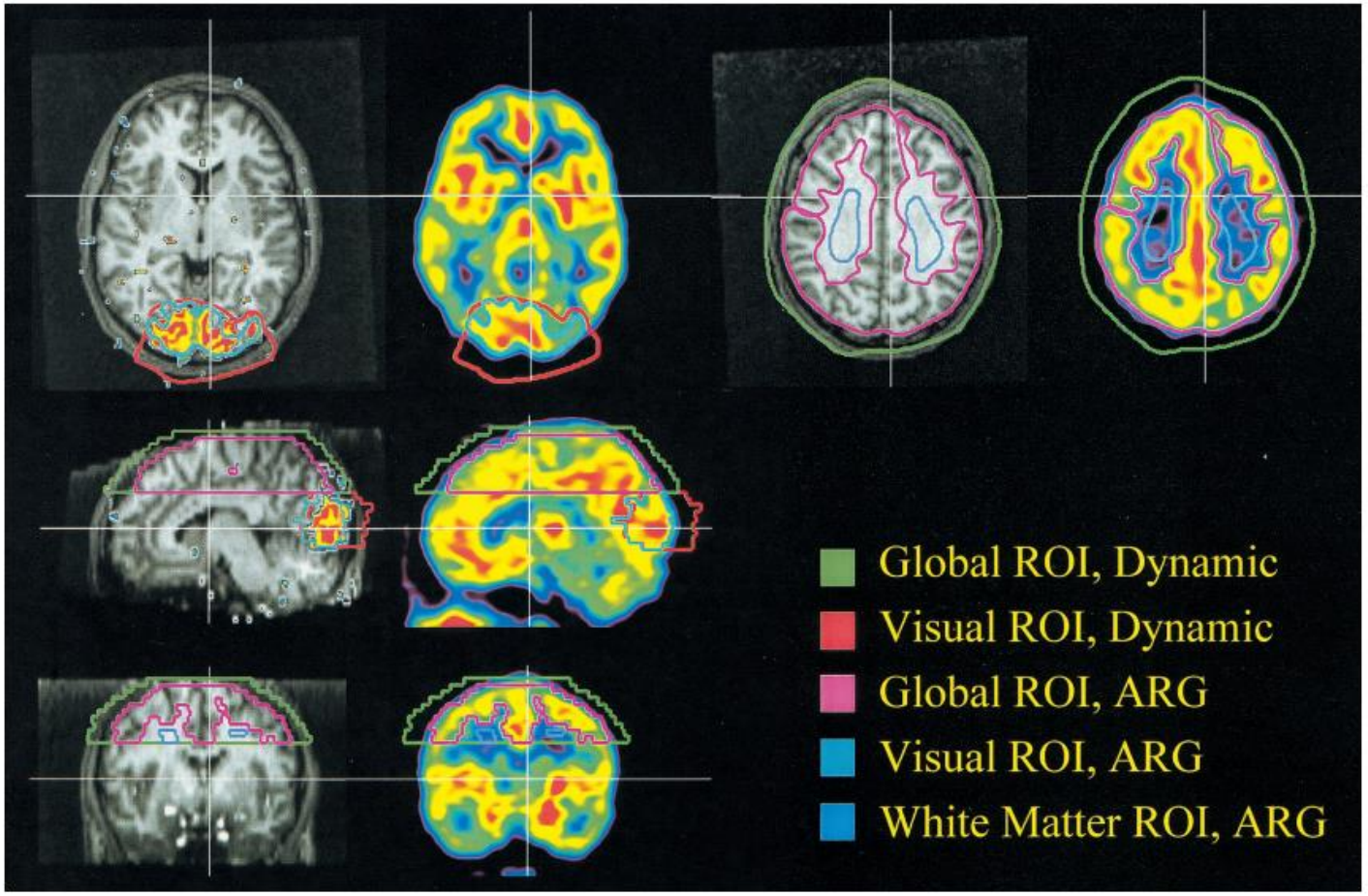

FIG 1. Configuration of visual, global, and white matter (autoradiographic only) regions of interest (ROIs) applied using either dynamic fitting or the autoradiographic method. The five ROIs are superimposed on a positron emission tomography autoradiographic regional cerebral blood flow (rCBF) image from a single subject and the corresponding coregistered T1-weighted magnetic resonance image with the significantly activated area ($P < 0.05$) during visual stimulation projected on top. Coronal, sagittal, and two transaxial views **(top)** are shown.

2000-Journal of Cerebral Blood Flow and Metabolism-law


Thanks for Your Kind Attention